

PHILOSOPHICAL TRANSACTIONS OF THE ROYAL SOCIETY A

MATHEMATICAL, PHYSICAL AND ENGINEERING SCIENCES

Transformation of organic matter in a Barents Sea sediment profile: coupled geochemical and microbiological processes

Journal:	<i>Philosophical Transactions A</i>
Manuscript ID	RSTA-2020-0223.R1
Article Type:	Research
Date Submitted by the Author:	14-Jul-2020
Complete List of Authors:	Stevenson, Mark; Newcastle University Faust, Johan; University of Leeds, Earth and Environment Andrade, Luiza; Newcastle University, School of Natural and Environmental Sciences Sales de Freitas, Felipe; University of Bristol, School of Earth Sciences Gray, Neil; Newcastle University, School of Natural and Environmental Sciences Tait, Karen; Plymouth Marine Laboratory Hendry, Katharine; University of Bristol, Earth Sciences Hilton, Robert; Durham University, Department of Geography Henley, Sian; University of Edinburgh School of GeoSciences, School of GeoSciences Tessin, Allyson; Kent State University, Department of Geology Leary, Peter; Newcastle University, School of Natural and Environmental Sciences Papadaki, Sonia; University of Bristol, School of Earth Sciences Ford, Ailbe; University of Leeds, School of Earth and Environment Maerz, Christian; University of Leeds Faculty of Environment, School of Earth and Environment Abbott, Geoffrey; Newcastle University
Issue Code (this should have already been entered and appear below the blue box, but please contact the Editorial Office if it is not present):	ARCTIC-CHANGE
Subject:	Environmental Chemistry (67) < CHEMISTRY (1002), Oceanography < EARTH SCIENCES, Geochemistry < EARTH SCIENCES, Biogeochemistry < EARTH SCIENCES, Geochemistry (78) < CHEMISTRY (1002)
Keywords:	Barents Sea, carbon cycling, microbial processes, geochemistry, marine sediment, organic matter reactivity

1
2
3
4
5
6
7
8
9
10
11
12
13
14
15
16
17
18
19
20
21
22
23
24
25
26
27
28
29
30
31
32
33
34
35
36
37
38
39
40
41
42
43
44
45
46
47
48
49
50
51
52
53
54
55
56
57
58
59
60



Author-supplied statements

Relevant information will appear here if provided.

Ethics

Does your article include research that required ethical approval or permits?:

This article does not present research with ethical considerations

Statement (if applicable):

CUST_IF_YES_ETHICS :No data available.

Data

It is a condition of publication that data, code and materials supporting your paper are made publicly available. Does your paper present new data?:

Yes

Statement (if applicable):

Data used in this study is available in the supplements.

Conflict of interest

I/We declare we have no competing interests

Statement (if applicable):

CUST_STATE_CONFLICT :No data available.

Authors' contributions

This paper has multiple authors and our individual contributions were as below

Statement (if applicable):

M.A.S. wrote the manuscript initial draft, conducted fieldwork/sampling, compiled datasets and carried out bulk and organic geochemical analyses. J.C.F. provided inorganic XRF data, conducted fieldwork/sampling, contributed ideas on sedimentology and to the initial manuscript. L.L.A. carried out microbiological analyses. F.S.F. advised on suitable organic geochemical techniques and provided insight into OM reactivity. N.D.G. designed microbiological approach and contributed key ideas on redox stratification to initial manuscript. K.T. carried out quantitative 16S rRNA analyses and co-designed microbiological approach. K.R.H project managed 14C radiocarbon analyses. R.G.H carried out $\delta^{15}\text{N}$ analyses with M.A.S. and advised on geochemical sampling strategy. S.F.H. & A.T. carried out fieldwork & porewater nutrient analysis which underpins model comparison. P.L. carried out bioinformatics and constructed sequencing pipeline. S.P. carried out 14C analyses on foraminifera. A.F. carried out grain size analysis. C.M. conducted fieldwork/sampling, advised on sedimentology and project managed inorganic geochemical aspects. G.D.A. contributed early ideas, revised the initial manuscript and project managed organic geochemical aspects. All authors commented on the manuscript and approved the final submission.

Transformation of organic matter in a Barents Sea sediment profile: coupled geochemical and microbiological processes

Mark A. Stevenson¹, Johan C. Faust², Luiza L. Andrade¹, Felipe S. Freitas³, Neil D. Gray¹, Karen Tait⁴, Katharine R. Hendry³, Robert G. Hilton⁵, Sian F. Henley⁶, Allyson Tessin⁷, Peter Leary¹, Sonia Papadaki³, Ailbe Ford², Christian März², Geoffrey D. Abbott¹

¹*School of Natural and Environmental Sciences, Newcastle University, Newcastle upon Tyne, NE1 7RU, UK*

²*School of Earth and Environment, University of Leeds, Leeds, LS2 9JT, UK*

³*School of Earth Sciences, University of Bristol, Bristol, BS8 1RJ, UK*

⁴*Plymouth Marine Laboratory, Prospect Place, Plymouth PL1 3DH, UK*

⁵*Durham University, Geography, Science Laboratories, South Road, Durham, DH1 3LE, UK*

⁶*School of GeoSciences, University of Edinburgh, James Hutton Road, Edinburgh EH9 3FE, UK*

⁷*Department of Geology, Kent State University, Kent, OH, 44240, USA*

Mark Stevenson DOI: 0000-0002-8955-0855

Geoffrey D. Abbott DOI: 0000-0001-9803-8215

Neil Gray DOI: 0000-0002-2395-4320

Katharine R. Hendry DOI 0000-0002-0790-5895

Felipe S. Freitas DOI: 0000-0001-8279-5772

Keywords: Barents Sea, carbon cycling, microbial processes, geochemistry, marine sediment, organic matter reactivity.

Summary

Process-based, mechanistic investigations of organic matter transformation and diagenesis directly beneath the sediment-water interface in Arctic continental shelves are vital as these regions are at greatest risk of future change. This is in part due to disruptions in benthic-pelagic coupling associated with ocean current change and sea ice retreat. Here we focus on a high-resolution, multi-disciplinary set of measurements that illustrate how microbial processes involved in the degradation of organic matter are directly coupled with inorganic and organic geochemical sediment properties (measured and modeled) as well as the extent/depth of bioturbation. We find direct links between aerobic processes, reactive organic carbon and highest abundances of bacteria and archaea in the uppermost layer (0-4.5 cm depth) followed by dominance of microbes involved in nitrate/nitrite and

*Author for correspondence (mark.stevenson@newcastle.ac.uk).

†Present address: School of Natural and Environmental Sciences, Newcastle University, Newcastle upon Tyne, NE1 7RU, UK

18 iron/manganese reduction across the oxic-anoxic redox boundary (~4.5-10.5 cm depth).
19 Sulfate reducers dominate in the deeper (~10.5-33 cm) anoxic sediments which is consistent
20 with the modeled reactive transport framework. Importantly, organic matter reactivity as
21 tracked by organic geochemical parameters (*n*-alkanes, *n*-alkanoic acids, *n*-alkanols and
22 sterols) changes most dramatically at and directly below the sediment-water interface
23 together with sedimentology and biological activity but remained relatively unchanged
24 across deeper changes in sedimentology.

26 Main Text

28 Introduction

29
30 Organic matter (OM) processing and transformation at the seafloor, ultimately drives the
31 sequestration of organic carbon and the biogeochemical modifications that occur prior to
32 long-term burial [1]. Across this important marine transition zone biological, geological and
33 physical processes take place at variable rates, including deposition of organic and inorganic
34 material, partial degradation of OM by microbes, sediment mixing by benthic fauna and,
35 dissolution and precipitation of mineral phases. Interactions between these coupled
36 processes are typically poorly characterised, but it is increasingly recognised that it is the
37 combined biogeochemical properties of sediments adjacent to OM that determine its
38 degradation and preservation trajectories [1], with alterations to the fate of deposited OM
39 particularly prevalent in high-latitude oceans. Arctic seafloor sediments are, sensitive to
40 changes in pelagic to benthic coupling as a result of alterations in the distribution of water
41 masses and sea-ice extent linked to climate changes [2], with process-based coupled
42 sedimentary organic-inorganic-microbial studies useful to capture the detail in the key
43 diagenetic processes and interactions which occur during OM transformation. It is also
44 important to distinguish external parameter changes that have impacts on organic carbon
45 reactivity from those that do not.

46
47 The OM at and below the Arctic shelf seafloor sustains a key ecological niche, including high
48 microbial diversity [3] and a rich benthic ecosystem [4]. Processing of organic carbon at the
49 seafloor is closely linked to water column productivity [5] and to delivery of algal biomass
50 from melting sea ice [6]. Over longer timescales marine organic carbon burial is the principal
51 mechanism of millennial scale carbon sequestration [7, 8] which, subject to processing and
52 transformation, becomes part of the geological record [9].

1
2
3
4
5
6
7 54 OM deposited at the seafloor undergoes intensive diagenetic transformation, with up to
8 55 ~99% degraded at the sediment-water interface (SWI), escaping long-term burial [10]. At
9 56 the SWI, the extent of transformation of OM results from the complex interactions between
10 57 OM composition and its stability to processing (e.g. redox conditions, microbial community
11 58 structure, mineralogy) [11, 12]. Consequently, such interactions result in distinct OM
12 59 reactivity changes during burial and differences in the rates of early diagenesis between
13 60 autochthonous (typically more reactive) and allochthonous sources (typically less reactive)
14 61 [13]. OM which 'survives' the uppermost sediment layer is subject to further microbial
15 62 activity where polymer hydrolysis, iron and manganese reduction, denitrification, nitrate
16 63 dissimilation, sulfate reduction and methanogenesis take place. Microbes indicative of these
17 64 processes inhabit often clearly stratified communities [14-16]. As OM is gradually broken
18 65 down, only the least reactive OM is left behind [17]. Redox processes, whereby sediments
19 66 transition from oxic to anoxic conditions, are an additional control on OM reactivity as
20 67 anaerobes inhabiting oxygen-free environments are limited in their ability to hydrolyze
21 68 more structurally complex compounds [10]. Simultaneously, bioturbating animals which
22 69 burrow into and physically mix sediments help control the thickness of the oxic layer,
23 70 regulating the amount and quality of organic carbon accumulated [18].
24
25
26
27
28
29
30
31
32
33
34

35 72 We selected the Barents Sea seafloor as our study location because it is characterised by a
36 73 mix of marine and terrestrial organic matter input, a clearly defined sequence of microbially
37 74 controlled redox zones, a variable input of inorganic material from land, and a strong
38 75 seasonality that affects chemical, physical and biological processes in a predictable manner.
39 76 The Barents Sea is also known to be vulnerable to climate change, with the existing extent of
40 77 sea ice loss expected to intensify in Arctic regions over the coming decades [19-21]. As well
41 78 as having a clear impact on wider Earth system processes [22, 23], sea ice loss driven by
42 79 atmospheric and oceanic warming is modifying the timing and abundance of biological
43 80 productivity within the Barents Sea by altering water column stratification [24], including the
44 81 relative balance of Arctic and Atlantic water masses [25], potentially altering the type of OM
45 82 delivered to the seafloor.
46
47
48
49
50
51
52

53 84 Although previous studies have combined microbiological and geochemical measurements
54 85 in Arctic continental shelf settings, they tend to focus on surface sediment transects [26],
55 86 down-core at low-resolution in deeper sediments [15, 16, 27, 28], or were limited by
56 87 sequencing libraries and study location [14], and so unable to show so clearly the depth-

88 successional redox transition close to the SWI. By using these techniques in tandem, it is
89 possible to fully explore the microbiological and geochemical basis underpinning diagenetic
90 models [29] highlighting the complexity of these processes and enabling quantification.

91
92 The main objective of this study is to improve our understanding of the interactions that
93 regulate and mediate OM processing at and below the SWI, by combining downcore
94 organic, inorganic and microbial measurements from the north western Barents Sea. We aim
95 to link biological and mineralogical mediated geochemical changes, by providing insight
96 into the reactivity of OM as a function of down-core trends in the context of microbial
97 abundances and activities related to redox processes. Overall, we expected that the
98 uppermost sediments would show evidence of a rapid decrease in the reactivity of OM
99 associated with the oxic layer, aerobic microbial activity, and biological sediment mixing (the
100 bioturbated layer). Beneath, we used our set of multi-disciplinary measurements to assess
101 the extent to which highly reactive carbon inputs are mineralised before cessation of aerobic
102 processes, and whether reactive carbon survives the transition to anoxia. We include
103 inorganic geochemical and grain size measurements to assess how changes in
104 sedimentation over the later Holocene affect trends in organic geochemical parameters.

105 106 **Methods**

107 108 **i) Study sites and sampling**

109
110 Two sediment cores from the same location (B15) were obtained during the JR16006 cruise
111 (2017) of the RRS James Clark Ross in the Barents Sea [30] and included multicore sampling
112 from station B15 E144 (78.25169 °N; 30.00909 °E) for depth resolved organic geochemistry
113 [31], microbial abundances and community compositions, and B15 E146 (78.25152 °N;
114 30.00849 °E) for inorganic geochemistry, to 33 cm depth (Supplements: Table S1). Station
115 B15 is located to the east of Svalbard's Edge Island and south of the island of Kongsoya
116 (Supplements: SI Fig. 1) and was sea-ice-covered during sampling [32]. The sediments were
117 taken from 315 m water depth in a glacial trough. Cores were sectioned at 0.5 cm intervals
118 to 2 cm depth and at 1 cm intervals to the base of the core. Sections were stored and flash
119 frozen in combusted foil (organic geochemistry (flash frozen -80 °C, stored -20 °C)), plastic
120 bags (inorganic geochemistry (-20 °C)), and plastic vials (microbiology (-80 °C)).

121 122 **ii) Bulk organic geochemistry**

123
124
125
126
127
128
129
130
131
132
133
134
135
136
137
138
139
140
141
142
143
144
145
146
147
148
149
150
151
152
153
154
155
156
157
158
159
160
Phil. Trans. R. Soc. A.

1
2
3
4
5
6
7 123
8
9 124 Total organic carbon (TOC) was analysed on freeze-dried acidified sediments (HCl; 4M; 4 h),
10 125 dried overnight (60 °C) and analysed with a CS230 Carbon/Sulfur Determinator (Leco
11 126 Corporation, Michigan, USA) using porous crucibles. The TOC content is expressed as the
12 127 weight percentage of dried sediment (wt.%). Nitrogen measurements were made using a
13 128 Vario MAX CNS analyser (Elementar, Langensfeld, Germany). TOC:N ratios were not
14 129 corrected for the molar weight of C and N. Stable nitrogen isotope measurements ($\delta^{15}\text{N}$)
15 130 were performed using an ECS 4010 Elemental Analyser (Costech Analytical Technologies
16 131 Inc., Valencia, CA) coupled to a Delta V Advantage (Thermo Finnigan, Hemel Hempstead, UK)
17 132 isotope ratio mass spectrometer and are reported in (δ) notation in per mille (‰) relative to
18 133 atmospheric N_2 (AIR). Sample precision was <0.2‰.
19 134

25 135 **iii) Grain size analysis**

26 136
27 137 Bulk sediment samples were disaggregated in an ultrasonic bath (15 minutes) and analysed
28 138 on a Mastersizer 2000E laser diffractometer for particles of a diameter range 0.1-1000 μm at
29 139 the University of Leeds. Results were categorised into 6 size fractions and are presented as
30 140 cumulative volume percentages.
31 141

32 142 **iv) Molecular organic geochemistry**

33 143
34 144 Lipids were extracted and analysed in a similar method to Holtvoeth *et al.* [33]. Briefly,
35 145 freeze-dried sediment (3-4 g) spiked with internal extraction standard (5 α -androstane) was
36 146 sonicated in dichloromethane: methanol (9:1 v/v) three times (15 mins each), with the
37 147 resulting total lipid extract (TLE) concentrated, left overnight in the presence of activated
38 148 copper to remove sulfur and passed through an anhydrous sodium sulfate column to
39 149 remove water. Transmethylation was performed by adding acetyl chloride in methanol (1:30
40 150 v/v) at 45 °C, left overnight and followed by a clean-up step with potassium carbonate to
41 151 neutralise excess acids. Prior to analysis, derivatisation of compounds containing hydroxyl
42 152 groups was performed using N,O-bis(trimethylsilyl)trifluoroacetamide (BSTFA) with 1%
43 153 trimethylchlorosilane (TMS) at 65 °C for 1 h.
44 154

45 155 Samples were injected (1 μl) into an Agilent 7890B Gas Chromatograph (GC) coupled to a
46 156 5977B MSD Mass Spectrometer (MS) operated in full scan mode (70 eV; source temp 230 °C;

47
48
49
50
51
52
53
54
55
56
57
58
59
60 *Phil. Trans. R. Soc. A.*

1
2
3
4 157 helium flow rate 1 mL/min). A 60 m J&W Scientific HP-1ms fused silica capillary column was
5 158 used for GC separation (0.25 mm x 0.25 μ m) with an oven temperature of 6 °C/min to 170
6 159 °C; hold of 1 min; followed by a slower ramp of 2.5 °C/min to 315 °C and a hold of 22 min.
7 160 Compounds were identified from their respective mass spectra and retention times, with
8 161 quantities calculated relative to the peak area of the internal standard 5 α -androstane and an
9 162 assumption of a 1:1 response.
10 163

11 164 For *n*-alkanoic acids parameters include total FAMES (fatty acid methyl esters), ratio of the
12 165 C₁₅ anteiso/C₁₆ FAME, terrigenous to aquatic fatty acid ratio (TAR_{FA}) [34] and total carbon
13 166 preference index (CPI_T) [35]. For sterols parameters include cholesterol/brassicasterol,
14 167 cholesterol/ β -sitosterol, stigmasterol/stigmastanol and β -sitosterol/stigmastanol. For *n*-
15 168 alkanes parameters were carbon preference index (CPI) [36] and odd over even
16 169 predominance for *n*-C₁₇₋₂₁ & *n*-C₂₁₋₂₅ (OEP₁₇₋₂₁ & ₂₁₋₂₅) [37]. Terrestrial to aquatic ratio (TAR)
17 170 and Aut/All (autochthonous/allochthonous) ratio was selected for *n*-alkanols [38]. Error
18 171 displayed is the standard deviation of a sample analysed in triplicate.
19 172

20 173 **v) Inorganic geochemistry**

21 174
22 175 X-ray fluorescence (XRF) was performed on freeze dried and gently grinded sediment
23 176 samples (700 mg) from B15 E146, mixed with di-lithiumtetraborate (4200 mg, Li₂B₄O₇,
24 177 Spectromelt A10), preoxidized at 500 °C with 1.0 g NH₄NO₃ (p.a.) and fused to homogenous
25 178 glass beads. Samples were analysed using a PW-2400 WD-XRF Scanner (Philips,
26 179 Netherlands) calibrated with geostandards at the University of Oldenburg with Fe, P and Mn
27 180 used in this study. Analytical precision and accuracy was <5%.
28 181

29 182 **vi) Microbiology**

30 183
31 184 Genomic DNA was extracted using the DNeasy® PowerSoil® kit (QIAGEN, Hilden,
32 185 Germany). Concentration and viability were tested using Qubit™ (Thermo Fisher Scientific,
33 186 Waltham, Massachusetts, USA) and polymerase chain reaction (PCR) respectively, prior to
34 187 sequencing. High throughput DNA sequencing was performed by the NUomics sequencing
35 188 service at Northumbria University (UK). 16S rRNA gene libraries were prepared following
36 189 protocol [39], in which each fragment was composed by an Illumina adapter, followed by an
37 190 index sequence (only for forward primer), a 10-nt pad to avoid formation of hairpin
38 191 structures, linkers and the V4 region specific either forward or the reverse primer. Primers
39
40
41
42
43
44
45
46
47
48
49
50
51
52
53
54
55
56
57
58
59
60

1
2
3
4
5
6
7 192 used were 4515F (GTGYCAGCMGCCGCGGTAA) and 806R (GGACTACHVGGGTWTCTAAT) as
8
9 193 per the Earth Microbiome Project protocol [40]. Sequencing was performed on the MiSeq
10 194 Personal Sequencer (Illumina, San Diego, CA, USA) using the V2 500 reagent kit.
11
12 195 Demultiplexed paired end FASTQ files were analysed using QIIME2 [41] using a pipeline
13 196 (<https://github.com/peterleary/markergene>). Amplicon sequence variants were generated in
14
15 197 QIIME2 using DADA2 [42] and taxonomy was classified using the SILVA 132 reference
16 198 database [43]. Taxonomic abundance data is expressed as percentage abundance (%)
17
18 199 enumerated from fractional abundances in sample libraries.
19
20

21 201 Quantitative PCR (qPCR) was used to determine the abundance of archaeal and bacterial
22 202 16S rRNA genes using the following primer pairs: Parch519F (CAGCCGCCGCGGTAA) and
23 203 ARC915R (GTGCTCCCCCGCCAATTCCT) [44] for archaea and Bact1369F
24 204 (CGGTGAATACGTTTCY-CGG) and Prok1492R (GGWTACCTTGTTACGACTT) [45] for bacteria
25 205 using primer concentrations and qPCR cycling conditions described in [46] and a LightCycler
26 206 96 instrument (Roche Life Science, Penzberg, Germany). Assays contained a standard curve
27 207 ranging from 10^2 to 10^8 amplicons μl^{-1} using cloned sequences. rRNA numbers were
28 208 quantified via comparison to standard curves using the Lightcycler 96 detection software.
29 209 No-template controls were below the threshold in all experiments. Measurements of 16S
30 210 rRNA for bacteria and archaea are presented as copies of genes per gram/wet weight
31
32 211 sediment.
33
34
35
36
37
38

39 213 **vii) Complementary measurements and datasets**

40
41 214

42 215 To provide constraint on the long-term sedimentation rates at the study site (and provide a
43 216 temporal framework to interpret the results) radiocarbon measurements (^{14}C -AMS) were
44 217 carried out on mixed foraminifera picked from samples at 27.5 cm depth, near the base of
45 218 the core. Sediment was dried, disaggregated, filtered and sieved ($>125\ \mu\text{m}$). Light
46 219 microscopy was used to pick and sort benthic and planktonic foraminifera tests for the Mini
47 220 Carbonate Dating System (MICADAS) (Ionplus, Dietikon, Switzerland) at the University of
48 221 Bristol. Measurements of ^{14}C were performed on both samples without graphitisation, but
49 222 with an acidification step, followed by analysis in the presence of a gas-ion source [47].
50 223 Bayesian calibration was carried out in MATLAB [48]. Acknowledging the challenges that
51 224 would be encountered by developing a sediment mass accumulation rate (MAR) on the
52 225 basis of a single point and its likely difference compared with a recent radionuclide
53
54
55
56
57
58
59

60 *Phil. Trans. R. Soc. A.*

226 approach [49], instead here we calculate percentage yr^{-1} TOC loss based on the youngest
227 basal age to provide an estimation and comparison of reactivity between oxic and anoxic
228 parts of the core.

229
230 We sourced empirical data on macrofaunal particle reworking from Solan *et al.* [50] based
231 on sediment profile imaging of introduced optically distinct particle tracers (luminophores)
232 to the surface of sediment cores after 12 days incubation [51]. Specifically, values for the
233 mean mixed depth ($f\text{-SPL}_{\text{mean}}$, time dependent indication of short term faunal mixing, [52])
234 and the maximum mixed depth ($f\text{-SPL}_{\text{max}}$, maximum vertical extent of faunal mixing [52]) are
235 presented alongside organic geochemical (Fig. 2) and microbial parameters (Fig. 3).

236
237 Porewater analysis of oxygen (O_2) was completed on sediment cores from the same station
238 (B15) in 2019 using a portable O_2 probe, with data sourced from Freitas *et al.* [29] and
239 presented against changes in microbial parameters (Fig. 3).

240
241 Modeled estimations of the relative contribution of metabolic pathways (aerobic respiration
242 ($\text{O}_2 - \text{M}$), denitrification ($\text{NO}_3 - \text{M}$), iron reduction ($\text{Fe}(\text{OH})_3 - \text{M}$), sulfate reduction ($\text{SO}_4 - \text{M}$)
243 and manganese reduction ($\text{MnO}_2 - \text{M}$) to based on reactive transport modelling are from
244 Freitas *et al.* [29] and are also presented against changes in microbial parameters (Fig. 3). We
245 additionally include model-derived oxygen concentration depth profiles (SI Fig. 2 & 3) [29].

246 247 **viii) Statistical analysis**

248
249 Data was explored for correlations between bulk variables, organic geochemistry,
250 geomicrobiology, porewater oxygen and modeled metabolic pathway processes, with
251 statistically significant relationships (using Pearson's correlation) listed in Fig. S2-S6.
252 Modeled datasets were resampled in Matlab (ver. R2019a) to the same depth intervals using
253 spline interpolation. Principal components analysis (PCA) was conducted due to short DCA
254 gradient lengths (< 2) in Canoco v4.51 [53] on \log_{10} transformed and centred data, with
255 samples highlighted in blue for proximity to the maximal extent of faunal reworking (Fig. 4).
256 Microbial taxa (defined by presence, absence and abundance), geochemical concentrations
257 and modeled percentage contribution of metabolic pathways to OM heterotrophic
258 degradation were included in the PCA table to create dissimilarity distances and eigenvalues
259 of the samples, with the two largest PCs plotted and superimposed over samples.

260

Results

An age-estimation was carried out at 27.5 cm depth with a mixed planktonic foraminifera ^{14}C -AMS age of 4075 ± 180 (1σ) ^{14}C year, calibrated to a median age of 4121 cal. yr BP (3632 to 4612 cal. yr BP, 95% confidence interval, Fig. 1). At the same depth, a paired mixed benthic foraminifera measurement gave a ^{14}C -AMS age of 5079 ± 91 (1σ) ^{14}C , calibrated to a median age of 5433 cal. yr BP (5245 to 5630 cal. yr BP, 95% confidence interval). Differences in the shape of planktonic compared with benthic foraminifera make them susceptible to bioturbation and sedimentation at different rates, providing ^{14}C evidence of key processes taking place in this system.

TOC content declined from a maximum of 1.78 wt.% at ~2.5 cm to minima of 1.33 wt.% at ~10.5 cm and 1.28 wt.% at ~32.5 cm (Fig. 1). Total N followed a similar trend, declining rapidly from 0.23 wt.% at the top of the core to 0.17 wt.% by ~10.5 cm and 0.15 wt.% at the base (Fig. 1). The ratio of TOC:N fluctuated throughout the core but gradually increased as a function of burial depth trend from a minimum of 7.5 at the top of the core to a maximum of 9.2 close to the base. The nitrogen isotope ratio ($\delta^{15}\text{N}$) declined from a maximum of 7.1‰ at the top of the core to a minimum of 5.8‰ at the base.

Profiles of total Fe and P concentrations displayed similar trends but with different magnitudes and were stable (5.1-5.6% and 0.16-0.17%, respectively) from the SWI to ~9.5 cm, below this depth, Fe and P increases to a maximum of 8.4% Fe and 0.3% P at a clear peak by ~14.5 cm. Below this peak Fe and P sharply declined to minimum values by ~16.5 cm with Fe ranging from 4.3% to 5.0% and P ranging from 0.11% to 0.13% to the bottom of the core. Total Mn was highest in the upper part of the core, peaking at ~4.5 cm at 1.02% and again at 8.5 cm to 0.96%, followed by a decline to low concentrations by ~10.5 cm which remained low to the base of the core.

Grain size was dominated by clay and silt from the top of the core (cumulative <63 μm fraction ~78%) to ~0.75 cm where coarser particles >63 μm (mainly fine sands) accounted for ~82% of the fraction until ~2.5 cm where finer particulates again dominated (<63 μm fraction >89%) (Fig. 1). Finer silts then decreased to < 16% (<63 μm fraction) by 5.5 cm, with a marked increase at ~14.5 cm to ~53 % coincident with Fe and P peaks. By ~19.5 cm finer

1
2
3
4 294 silts returned to previous levels <16% (<63 μm fraction), before a gradual rise from ~24 cm,
5 295 peaking at ~90% from ~30.5 cm to the base of the core.
6
7 296

8
9 297 Organic geochemical ratios of key compounds displayed clear changes in the uppermost
10 298 ~9.5 cm of the core, with the most pronounced changes coincident with maximum
11 299 bioturbation in the top ~4.5 cm (4.3 cm is greatest of three maximum bioturbation
12 300 replicates [50]) (Fig. 2). Some compounds had especially pronounced changes in the
13 301 uppermost sample coincident with mean bioturbation at 0.5 cm (0.5 cm is the average of
14 302 three mean bioturbation replicates [50]). Total FAMEs declined rapidly from >1400 $\mu\text{g g}^{-1}$
15 303 TOC at 0.5 cm to ~200 $\mu\text{g g}^{-1}$ TOC at ~2 cm, with subsequent values ranging narrowly
16 304 between ~200 and 500 $\mu\text{g g}^{-1}$ TOC to the base (Fig. 2). The ratio of C_{15} anteiso: C_{16} FAME, an
17 305 indicator of microbial activity, was high in samples just below the sediment surface, within
18 306 maximum bioturbation (0-4.3 cm) from ~0.75-2.5 cm with values 0.15-0.19 and also at ~5.5
19 307 cm with a value of 0.18, followed by a general declining trend to ~25.5 cm (0.06). TAR_{FA}
20 308 increased from a minimum of ~0.1 at the top of the core to a maximum of ~1.2 at ~1.75 cm
21 309 within the zone of maximum bioturbation. The CPI_T ratio for *n*-alkanoic acids was high in the
22 310 uppermost sample (~13.5) coincident with mean bioturbation, declining to fluctuations
23 311 between ~5 and 9.4 to the base.
24 312

25 313 The ratio of cholesterol/brassicasterol was low at the top of the core (<1.3), increasing to ~3
26 314 (2.5 cm) within the zone of bioturbation, before decreasing to <1.8 by ~3.5 cm, with a
27 315 further peak to ~2.4 at ~9.5 cm. Similarly, cholesterol/ β -sitosterol also peaked at ~2.5 cm
28 316 depth (to >4), prior to a general decrease to the base of the core (<1.3). In contrast,
29 317 stigmasterol/stigmastanol declined from a maximum of 1.0 at the top of the core to 0.2 at
30 318 ~9.5 cm, followed by fluctuations between 0.1 and 0.4 to the base. Similarly, the ratio of
31 319 sterols β -sitosterol/stigmastanol declined rapidly from a peak of 4.2 at the top of the core to
32 320 ~1.2 by ~9.5 cm, remaining stable to the base of the core (1.4 to 0.9). The CPI ratio for *n*-
33 321 alkanes declined from a maximum of 2.5 at the top of the core to 1.7 at a depth of ~9.5 cm
34 322 below the seafloor. With further increase in burial depth to ~17.5 cm, there was a
35 323 subsequent smaller increase in CPI with values for deeper horizons below this ranging from
36 324 1.9 to 1.7. The OEP for *n*-alkanes from C_{21} - C_{25} ranged from a maximum of 1.6 at the top of
37 325 the core to a minimum of 1.1 by ~3.5 cm, with values below this fluctuating between 1.1 and
38 326 1.2. OEP for *n*-alkanes C_{21-25} were especially prominent in the uppermost sample (~1.6)
39 327 coincident with mean bioturbation, with all values below this <1.3. The TAR index for *n*-
40 328 alkanes increased from a maximum of ~1 at the top of the core to >4 at ~9.5 cm, prior to
41
42
43
44
45
46
47
48
49
50
51
52
53
54
55
56
57
58
59
60

1
2
3
4
5
6
7 329 fluctuations between ~2 and ~3.3 to the base. The autochthonous/allochthonous ratio for
8 330 *n*-alkanols also showed a decline in the uppermost layer from a maximum of 0.9 at the top
9 331 of the core to a minimum of 0.4 by ~9.5 cm.

10 332
11 333 16S rRNA gene counts representative of bacterial and archaeal cell numbers fluctuated but
12 334 were present in abundance from the SWI down to ~11.5 cm, below which abundances were
13 335 orders of magnitude lower (Fig. 3). For bacterial 16S rRNA genes above 11.5 cm the mean
14 336 was 3.32×10^7 copies g^{-1} wet sediment, declining markedly to 9.23×10^5 copies g^{-1} wet
15 337 sediment below 11.5 cm, while for archaea the mean above 11.5 cm was 7.28×10^7 copies g^{-1}
16 338 wet sediment declining to 2.31×10^6 copies g^{-1} wet sediment (Fig. 3). The greatest peaks in
17 339 bacterial and archaeal 16S rRNA genes were within the uppermost ~4.5 cm coincident with
18 340 most intense bioturbation. The progressive decline in these numbers could either be
19 341 attributable to the balance between depositional inputs at the surface and subsequent
20 342 death and cell lysis with sedimentation, or may relate to in-situ growth. Based on 16S rRNA
21 343 gene sequence analysis these depth related declines in absolute abundances were
22 344 accompanied by distinctive successional changes in the relative abundances of some
23 345 dominant archaeal and bacterial taxa indicative of a depth related transition from aerobic to
24 346 anaerobic microbial processes, linked to bioturbation depth. For instance, 16S rRNA gene
25 347 sequences related to the BD7-8 marine group [54] declined sharply from a maximum of
26 348 2.36% of sequences in the amplicon library at the top of the core to 0% by ~5.5 cm, with
27 349 only minor occurrences in amplicon libraries from depths below this (Fig. 3). Group BD7-8 is
28 350 considered cosmopolitan in marine benthic habitats and are putative aerobic and nitrate
29 351 reducing mixotrophs [55, 56]. Declines in group BD7-8 were coincident with both decreases
30 352 in measured ($R=0.97$, $p < 0.01$) and modeled ($R = 0.94$, $p < 0.01$) O_2 concentration depth-
31 353 profiles (Supplements; Figure S2) and the zone of bioturbation (Fig. 3). Highlighting links
32 354 between organic matter quality and aerobic processes, there were positive correlations
33 355 between CPI for *n*-alkanes and both measured ($R = 0.81$, $p < 0.05$) and modeled ($R= 0.92$, p
34 356 < 0.01) O_2 concentration depth-profiles (Supplements, Figure S2). Similar positive
35 357 correlations between modeled relative oxygen contribution, $\delta^{15}\text{N}$ ($R = 0.89$, $p < 0.01$), %N (R
36 358 $= 0.93$, $p < 0.01$) and %TOC ($R = 0.86$, $p < 0.01$) were found, with similar but slightly weaker
37 359 correlations between model-derived O_2 concentration depth-profiles and $\delta^{15}\text{N}$ ($R = 0.83$, $p <$
38 360 0.01), %N ($R = 0.88$, $p < 0.01$) and %TOC ($R = 0.84$, $p < 0.01$) (Supplements; Figure S3).
39 361 Corroborative of the presence and depth related consumption of molecular oxygen in the
40 362 upper few cm (above ~9.5 cm) of the sediment, sequences related to aerobic ammonia

oxidizers from the family *Nitrosopumilaceae* [57] followed a general declining trend from the top of the core to the base, although their abundance varied (Fig. 3). *Nitrosopumilaceae* was negatively correlated with TOC:N ratio ($R = 0.62$, $P < 0.01$) and positively correlated with $\delta^{15}\text{N}$ ($R = 0.91$, $p < 0.01$) (Supplements; Figure S4).

In contrast to these depth related declines, sequences related to the putatively iron reducing *Shewanellaceae* family [58] which variably increased their abundance in amplicon libraries were persistent up to ~10.5 cm (Fig. 3). Similarly, sequences related to the *Desulfuromonadales* family (also putatively capable of iron reduction [59]) generally increased their relative abundances up to ~10.5 cm but with an additional peak at ~15.5 cm. Likewise, sequences related to the family *Methylomirabilaceae* (capable of methane oxidation coupled to nitrite reduction [60]) increased in abundance at the top of the core peaking at 14.1% of the amplicon library at 10.5 cm. In a similar region of the core, sequences of the *Brocadiales* group (involved in anammox by ammonia oxidation linked to nitrate/nitrite reduction [61]) were at highest sustained abundance between 5.5 and 10.5 cm (Fig. 3). All four of these groups had varying associations with modeled relative denitrification contribution. The strongest relationship was with *Brocadiales* ($R = 0.74$, $p < 0.01$), followed by *Methylomirabilaceae* ($R = 0.57$, $p < 0.01$), *Shewanellaceae* ($R = 0.53$, $p < 0.01$) and *Desulfuromonadales* ($R = 0.45$, $p < 0.01$) (Supplements; Figure S5). In contrast to all of the other taxa detailed above, sequences related to the sulfate reducing *Desulfobacteraceae* [62]) were largely absent above ~10.5 cm (Fig. 3). The presence of *Desulfobacteraceae* continued below this oxic-anoxic transition to the base of the core and was closely correlated with modeled relative sulfate reduction contribution ($R = 0.88$, $p < 0.01$) (Supplements; Fig. S6).

The PCA ordination biplot provides insight into co-associations between geochemical, geomicrobial, modeled relative metabolic pathways and bioturbation datasets (Fig. 4). For example, the assemblage to the right part of the biplot is closest in ordination space to the uppermost core samples in the oxic and bioturbated zone which includes modeled and measured O_2 , Arctic marine cosmopolitan aerobic marine group BD7-8, measurements of bacterial and archaeal 16S rRNA gene abundance and Mn. All organic geochemical variables (sterols, *n*-alkanes, *n*-alkanols and *n*-alkanoic acids) and $\delta^{15}\text{N}$ appear to co-vary and are grouped at the lower right part of the biplot. In contrast, *Desulfobacteraceae*, $\text{SO}_4 - \text{M}$, $\text{Fe}(\text{OH})_3 - \text{M}$, TOC:N and TOC are present towards the lower left part of the biplot. To the top left of the biplot, $\text{NO}_3 - \text{M}$ and $\text{MnO}_2 - \text{M}$ are grouped, with *Brocadiales*, Fe, P,

1
2
3
4
5
6
7 398 *Methylomirabilaceae*, *Desulfuromonadales*, *Nitrosopumilaceae* and *Shewanellaceae* grouped
8
9 399 towards the top of the right quadrant. PCA axis 1 decreased from a maximum of ~2 at the
10 400 top of the core clearly to a minimum of ~ -0.5 by ~7.5 cm, highlighting changes initially in
11 401 indicators sensitive to the oxic interface (e.g. organic geochemistry, BD7-8, 16S
12 402 archaea/bacteria), below which variance fluctuated (Supplements; Fig. S7). PCA axis 2
13 403 featured an initial peak in the oxic zone (~1.2 at 1.25 cm), a decrease (-0.2 by 4.5 cm), and
14 404 then a peak to ~2 by 6.5 cm coincident with fluctuations in multiple sequenced microbial
15 405 indicators, below which variance fluctuated to the base.
16
17
18
19
20

21 407 **Discussion**

22 408
23
24 409 We examine evidence for changes in OM reactivity with depth below the seafloor across the
25 410 redox succession and assess the influence of changes in sedimentology on the reactivity of
26 411 OM, to provide new insight on the coupling between geochemical and microbiological
27 412 processes in Arctic shelf sea carbon cycling.
28
29
30

31 413
32 414 There are clear changes in bulk parameters (~10 cm) as well as biomarker distributions (~4.5
33 415 cm) in the uppermost part of the core (Fig. 1 & 2), with coincident declines in aerobic
34 416 microbiological proxies (Fig. 3). Changes closest to the SWI are consistent with extensive
35 417 transformations of OM in the aerobic and bioturbated sediment layer [10, 63, 64]. Below the
36 418 aerobic zone, the most reactive OM has been largely consumed with clear deeper
37 419 succession of microbes indicative of a transition to anoxia. This is evidenced by microbes
38 420 capable of iron, manganese and nitrite dependent methane oxidation (~4.5 - 10.5 cm),
39 421 transitioning at greater depth to sulfate reduction in these deeper sediments (~10.5-33 cm)
40 422 where OM is less reactive (Fig. 3). Despite bioturbation levels being consistent with regional
41 423 [65] and local [50] studies (i.e. maximal depth of faunal mixing ~4.3 cm), these results
42 424 provide clear evidence of distinct successional redox zones transitioning with depth and
43 425 associated stratification of microbial community composition [15] coupled to the diagenesis
44 426 of reactive carbon, but at a reduced capacity.
45
46
47
48
49
50
51

52 427 53 428 **i) Organic matter transformation and diagenesis below the SWI**

54 429
55
56 430 As well as the decrease in bulk TOC and N in the uppermost ~10 cm, changes inferred by
57 431 molecular organic geochemical parameters indicate a rapid decrease in the reactivity of OM

58
59
60 *Phil. Trans. R. Soc. A.*

(Fig. 2). The most pronounced changes (top ~4.5 cm) are coincident with the extent of bioturbation [50]. A marked decrease in the ratio of β -sitosterol/stigmastanol can be explained by the mechanism of hydrogenation [66] and decreases in the ratio of stigmasterol/stigmastanol by reduction reactions [67]. Such reactions are also observed in the transformation and diagenesis of all sterols [68]. Although some sterols, such as β -sitosterol and stigmasterol, can be of a terrestrial plant origin [69], in this location in sediments with a mixed but mainly marine signature [31] sterols could also have a marine origin [70]. The CPI index for *n*-alkanes also shows a marked decline in the uppermost sediments, which reflects OM diagenesis as the more abundant odd chain lengths degrade [71]. This is mirrored by declines from the uppermost sample in *n*-alkanoic acid CPI_T index (where the more abundant even compounds degrade) [35] and pronounced decreases in the concentration of these compounds. Although changes in the mixing or delivery of terrestrial OM can result in changes in CPI [72], the low values in these sediments suggest a mixed, but primarily marine signature.

Coincident with CPI decreases, OEP for *n*-alkanes in the range C_{17} - C_{21} and C_{21} - C_{25} also decline, with marked changes between the sample at the SWI (~ 0.5 cm) and deeper sediment layers [37]. With decreases in OEP, OM rapidly becomes degraded and less bioavailable, a process which is most pronounced close to the SWI. Similarly, for the more labile *n*-alkanols, changes in the ratio of autochthonous to allochthonous-derived compounds [38] in the uppermost layer indicate active processing of compounds in the organic rich layer. A reverse trend in the *n*-alkanol TAR ratio probably can be explained to ~4.5 cm by dilution by more abundant short chain compounds close to the SWI, which are also less resistant to degradation than longer chain compounds [73]. However, increases to the TAR *n*-alkanol values to ~5 at ~9.5 cm could point to past deposition of OM, which appears to be reflected by increases in CPI_T for *n*-alkanoic acids and the ratio of cholesterol/brassicasterol. The pulse in TAR for *n*-alkanoic acids at ~1.75 cm suggests delivery of terrestrial material is unlikely to have been consistent and likely varied over time. Overall, the changes close to the SWI reflect the early diagenesis of lipid biomarkers observed in the oxic layer of ocean sediments [13] and are coincident with observed bioturbation zone [50], while also highlight an underlying terrestrial influence [29, 74].

Loss of TOC with depth (Fig. 1) is markedly more pronounced in the oxic layer compared with the anoxic sediments (indicated by the relative abundance of *Desulfobacteraceae*, in sequence libraries Fig. 3). For instance, TOC declines from a peak of ~1.8% close to the top

of the core at ~2.5 cm to ~1.3% by 10.5 cm at the base of the oxic zone, prior to the transitional zone indicated by *Desulforbacteraceae* (Fig. 3). Based on extrapolating the age estimation, this corresponds to a loss, given dating approximations of 3.8×10^{-4} % TOC per year. In marked contrast, in the established zone of anoxia from ~13.5 cm to the base, TOC declines from ~1.5 to ~1.3 over a longer time period corresponding to a loss of 8.4×10^{-5} % TOC per year. Although this estimation does not resolve changes in sedimentation rate and is based only on a basal age, the difference in relative TOC loss with depth corroborates changes in molecular proxies (*n*-alkanes, *n*-alkanols, sterols) which provides evidence that OM reactivity is greatest in the uppermost layer. Future changes in the relative position of the oxic/anoxic interface could lead to changes in carbon cycling driven by reactivity at the seafloor.

Both organic geochemistry (CPI *n*-alkanes, TOC, N, $\delta^{15}\text{N}$) and measured/modeled porewater O_2 in the uppermost layers are statistically correlated with declines in the proportion of the BD7-8 marine group (Fig. 3; Supplements Fig. S2 & 3), attributed to bacterial diversity in oxic marine sedimentary environments [54] and previously detected in surface sediments of the South Atlantic Ocean [75] and the western Arctic Ocean [76]. Although more variable, 16S rRNA data show that bacteria and archaea are also only present in abundance in the uppermost 0-9.5 cm mixed layer (Fig. 3). Bacterial and archaeal richness and abundance is known to decrease exponentially with depth [77, 78] and links between organic degradation and microbial activity are particularly pronounced close to the SWI [79]. Similarly, the highest consistent levels of *Nitrosopumilaceae* (capable of ammonia oxidation to nitrite [80]) are in the uppermost sediments, correlating with lower TOC:N ratios and higher $\delta^{15}\text{N}$ indicative of microbial activity (Supplements Fig. S4). Here, ammonia oxidising archaea utilise ammonia likely generated through OM mineralisation in the sediments below which diffuse up to the bioturbated, oxic zone. The ratio of C_{15} anteiso/ C_{16} FAMES is corroborated by extensive microbial activity just below the sediment-surface interface (Fig. 2), with this compound often linked to bacterial activity as they are major constituents of bacterial membrane lipids [81] and have been detected in aquatic environments [82] including ocean sediments [83]. Peaks in the ratio of cholesterol/brassicasterol and cholesterol/ β -sitosterol within the zone of bioturbation at ~2.5 cm have a similar explanation as cholesterol is a key component of bacterial membrane lipids [84]. Decreases in bulk $\delta^{15}\text{N}$ (Fig. 1) are probably explained by preferential degradation of compounds such as proteins rich in ^{15}N , deposited

1
2
3
4 500 at the SWI and subsequently degraded [64, 85], potentially sourced from under ice algal
5 501 blooms.

6 502

7 503 **ii) Stratification of microbes and geochemistry across the oxic to anoxic**
8 504 **interface**

9 505

10 506 Further changes linked to the processing of OM take place below the aerobic, bioturbated
11 507 zone. In the aerobic to anaerobic transition zone peaks in the relative abundance of
12 508 bacterial taxa *Desulfuromonadales* and *Shewanellaceae* from ~6.5 cm downwards indicate
13 509 that Fe³⁺ and Mn⁴⁺ reduction is taking place (Fig. 3) [86]. These taxa can utilise (reduce
14 510 through dissolution) metals such as Fe³⁺ and Mn⁴⁺ oxides as terminal electron acceptors.
15 511 *Shewanella spp.* are adapted to chemically stratified redox transitions [58]. Sediment Mn
16 512 concentrations also increase coincident with the two major peaks in *Desulfuromonadales* in
17 513 the oxic zone, suggesting that taxa capable of metal reduction are important close to the
18 514 redox transition (Fig. 3). Seasonal or decadal oscillations in the delivery of OM causing the
19 515 position of the redox boundary to fluctuate could be a process here, potentially explaining
20 516 the position of Mn at the upper part of the redox boundary based on kinetics of oxidation
21 517 and reduction [87]. The oxic to anoxic redox transition is most clearly illustrated by the
22 518 marked increase of *Desulfobacteraceae* from ~10.5 cm downwards which are known sulfate
23 519 reducers [88] and correlates with modeled sulfate reduction (Fig. 3; Supplements Fig. S6).
24 520 Sulfate reducing taxa are known to persist below the oxic layer, typically also below the
25 521 oxidants NO₃⁻, Fe³⁺ and Mn⁴⁺, where they are involved in the remineralisation of organic
26 522 carbon [89].

27 523

28 524 Coincident with the increase in sulfate-reducing taxa at and below the oxic-anoxic transition,
29 525 the abundance of methane oxidizing taxa evidenced by bacteria in the group
30 526 *Methylomirabilaceae* peaked markedly (Fig. 3). Based on amplicon library relative abundance
31 527 (15%) the *Methylomirabilis* are an important group in this sequence. This family have been
32 528 shown to participate in anaerobic methane oxidation linked to nitrate/nitrite reduction (via
33 529 the generation of molecular oxygen utilised by methane monooxygenase (MMO)) [90].
34 530 *Methylomirabilis* have been previously detected in ocean sediments [91], sub-Arctic lake
35 531 sediments [92] and are abundant in methane rich environments such as paddy fields [93].
36 532 On balance, the coincidence of this group with sequences related to the *Brocardiales*, which
37 533 are implicated in anammox (ammonia oxidation linked to nitrate/nitrite reduction [61]), may
38 534 suggest involvement in ammonia oxidation. Genomic studies have suggested the potential

39 535

40 536

41 537

42 538

43 539

44 540

45 541

for the oxidation of ammonia by *Methylomirabilis* by use of their oxygen dependent MMO [90] rather than by the annamox pathway involving hydrazine production [61]. Increases in TOC:N ratio in the anoxic sediments and transition zone (Fig. 3) are probably explained in this system by microbial activity utilising more N, where this is limited and more labile than C, producing OM with TOC:N ratios ~10 which gradually dilutes the lower TOC:N ratio of phytoplankton derived matter, characteristic of the uppermost layer. Additionally, if *Methylomirabilis* is acting as an ammonia oxidiser it likely produces N₂ as an inert gas, likely resulting in the gradual loss of solid phase N down the core evidenced by increases in TOC:N ratios in the anoxic sediments. Many of these bacterial taxa have the potential to be involved in multiple processes at this key transition, but denitrification (Fig. 3) also appears to be particularly important at this key transition with associations between *Methylomirabilis*, *Brocardiales*, *Desulfuromonadales* and *Shewanellaceae* and modeled denitrification [29] (Supplements; Fig. S5).

iii) How does the reactivity of OM delivered to and preserved within sediments change across differences in sedimentology?

Fine particulates (silty clays) are abundant close to the SWI (Fig. 1), together with biomarkers which infer more reactive OM such as high CPI and OEP_(17-21 & 21-25) for *n*-alkanes, high ratios of stigmaterol/stigmastanol and β -sitosterol/stigmastanol, plus high total alkanolic acids (Fig. 2). Close to the SWI the weaker bonds of more reactive organic components may continue to be attached and the fine particulate (clay-like) minerals may help, in part entrain, enmesh or adsorb organics in a mineral matrix [94]. The coarser fraction immediately beneath from ~0.75 until 2.5 cm could be associated with bioturbation sorting and be a particle capture layer [95], immediately below the most intensive reworking zone. Finer particles from ~2.5 to 5.5 cm remain within the maximum bioturbation zone, with these size classes potentially supporting capture of microbially influenced biomarkers (e.g. pulses of C₁₅ anteiso:16:0 FAMES and cholesterol:brassicasterol ratios, Fig. 2) when evidence of microbial activity (e.g. 16s RNA archaea, Fig. 3) is high.

The transition to finer particulates peaking at ~14.5 cm, which is accompanied by increases in Fe and P (Fig. 1) could be a sediment deposition event similar to scenarios across the Barents Sea. Although the specific underlying mechanism driving this potential deposition cannot be disentangled from this evidence, possibilities include regional transport from land

Phil. Trans. R. Soc. A.

[96], cross-shelf transport [97] or accumulations linked to seasonal redox oscillations [87]. We might expect organic biomarker evidence of either source (e.g. terrestrial input) or reactivity changes to be coeval with this change in sedimentology, but there is little evidence of response at similar magnitudes to OM transformations at the SWI. Slight fluctuations in *n*-alkane CPI at ~17.5 cm and OEP₁₇₋₂₁ at ~15.5 cm (Fig. 2) could indicate slightly more reactive organics is being preserved in finer particulates, but the response is minor and offset slightly from changes in grain size. Since the change in sedimentology does not have a clear link with reactivity of OM evidenced by bulk parameters (TOC, N, TOC:N ratio) or biomarker distributions (*n*-alkanes, *n*-alkanols or sterol ratios) then this suggests the change in sedimentology was either not accompanied by significant organic material, or processes at the SWI have removed any noticeable geochemical signatures. Previous studies suggest the material released from ice sheets and glaciers are sources of quickly processed highly reactive OM [98, 99]. Potential reactive material, which may have been brought into the system during past disturbances or reworking may have been subsequently degraded, and does not continue to exert a major impact on OM cycling (evidenced by extractable lipid fractions), except by potentially supporting in part, microbial taxa capable of using metals for respiration (*Shewanellaceae* and *Desulfuromonadales*, Fig. 3). The Mn and Fe changes in sedimentology (Mn peak is shallower) may be offset due to different kinetics of oxidation and reduction between oxides of these compounds [87] and these microbes may also be sensitive to porewater diffusion of metals.

iv) The role of coupled microbial and geochemical studies for understanding carbon cycling in Arctic shelf systems

Clear separation between indicators of OM reactivity, microbial communities at the redox interface and indicators of sulfate reduction processes in the PCA biplot (Fig. 4), which vary across the redox profile (Supplements; Figure S7), highlights the coupled relationships between a multiplicity of complementary but competing processes which stratify according to depth. This clear separation supports close relationships between geochemical variables (e.g. CPI *n*-alkanes, $\delta^{15}\text{N}$, %N, %TOC) and O₂, beneath which across the oxic to anoxic transition microbes involved in multiple processes stratify (denitrification, nitrite production and iron/manganese reduction etc.), prior to evidence of sulfate reduction below the transition to depth (Supplements; Fig. S2 - 6).

1
2
3
4
5
6
7 603 This detailed geochemistry and microbiology study provides a coupled framework with
8 wider sedimentary processes including porewater geochemistry (from reactive transport
9 604 modelling and measured O₂ [29]) and bioturbation [50], consistent with expectations for a
10 605 continental shelf system [100]. The extent of successional redox associated processes
11 606 controlling the cycling of carbon in sediments at and below the SWI is coupled closely to
12 607 the environmental setting (Barents Sea continental shelf) and is likely to be sensitive to
13 608 future changes, especially those driven by atmospheric and oceanic warming. The trends in
14 609 OM transformations and redox succession observed at B15 are likely to be typical of shelf
15 610 environments with similar water depth, sediment type, overlying water masses and levels of
16 611 primary production and carbon export. Specifically, although this study focuses on one
17 612 station (B15) it is possible to suggest, broadly that this station may be representative of
18 613 wider regional processes. In terms of surface sediment particle size in the Barents Sea, this
19 614 station is consistent with locations in a southerly direction south (to ~ 75 °N) [101] and so
20 615 profiles may be similar across a wider part of the continental shelf. If upscaled, this study
21 616 would demonstrate there is a key pool of reactive OM dependent on microbial control,
22 617 making up part of the more reactive carbon burial component which could be lost from this
23 618 key store if the redox interface was shallower. This scenario is possible as changes in OM
24 619 supply are likely to adjust with future changes in ocean stratification and sea-ice retreat [25].
25 620
26 621

27 622 Future studies should follow a similar approach to assess how the depth and extent of redox
28 623 sensitive successional processes might be affected by geographical position across Arctic
29 624 continental shelves (e.g. Chukchi Sea, Bering Sea, East Siberian Sea, Laptev Sea).

30 625 Comparisons of profiles will be particularly insightful to help understand how changes to the
31 626 Arctic including sea ice losses and associated changes in water column vertical mixing [25,
32 627 102] are influencing ocean primary productivity in the Arctic [5], which is tightly coupled to
33 628 carbon fluxes reaching the seafloor [9]. Such studies will assess the stability and
34 629 bioavailability of carbon sequestered as organic carbon burial is the principal mechanism for
35 630 long-term carbon sequestration [7, 8], which ultimately becomes part of the permanent
36 631 geological record [9].
37 632

38 633 **Conclusions**

39 634
40 635 Our study demonstrates mechanistic links between microbial processing and changes in
41 636 organic and inorganic parameters across the oxic to anoxic interface are distinct, but

42
43
44
45
46
47
48
49
50
51
52
53
54
55
56
57
58
59
60 *Phil. Trans. R. Soc. A.*

1
2
3
4 637 interactive and tightly coupled to biological mixing and the reactivity of OM. Specifically we
5 638 found:

- 7 639 i) Distinct links between aerobic processes, reactive carbon and highest abundances
8 640 of bacteria and archaea in the uppermost layer (0-4.5 cm), coincident with the
9 641 extent of biological mixing and changes in the reactivity of OM (indicated by *n*-
10 642 alkanes, *n*-alkanols, *n*-alkanoic acids and sterols).
13 643 ii) A dominance of microbes involved in nitrate/nitrite and iron/manganese
14 644 reduction across the oxic-anoxic redox boundary (~4.5-10.5 cm), with convincing
15 645 denitrification relationships confirming this key intermediate zone.
18 646 iii) Sulfate reducers dominate in deeper anoxic sediments which is consistent with
19 647 OM transformations and biological reworking, but that deeper changes in
20 648 sedimentology have only minor effects on the reactivity of organic carbon
21 649 (compared with at the SWI), probably due to past processing.

24 650
25 651 Future research should compare coupled geochemistry-microbial profiles between ice-
26 652 covered and ice-free zones of the Arctic to elucidate linkages between ice cover and
27 653 microbial processing of OM at the seafloor. This is especially pertinent and should be
28 654 coupled with estimates of carbon burial in different locations across the Barents Sea, given
29 655 the trend for increasing oceanographic changes in this region [25].
30 656
31 657

36 658 Additional Information

39 660 **Acknowledgments**

40 661 Appreciation is given to the excellent support provided by the crew and science parties on
41 662 board the RRS James Clark Ross (JR16006) including shipboard facilities (NOC & BAS) and
42 663 PSO Jo Hopkins. We thank Heather Birch and Timothy Knowles for assistance with ¹⁴C-AMS
43 664 dating of foraminifera, Martin Solan for provision of bioturbation metrics and Jeff Peakcall
44 665 for providing access to a grain size analyser. We appreciate technical assistance from Darren
45 666 Gröcke (IRMS), Bernard Bowler (EA), Alex Charlton (TOC) and Paul Donohoe (GC-MS). We
46 667 are grateful for the comments from the reviewers, which helped improve the manuscript.
47 668

51 669 **Funding Statement**

52 670 This work resulted from the ChAOS project (NE/P00637X/1; NE/P006493/1; NE/P006108/1;
53 671 NE/P005942/1) part of the Changing Arctic Ocean programme, funded by UKRI Natural
54 672 Environment Research Council (NERC).
55 673

Data Accessibility

Data used in this study is available in the supplements.

Competing Interests

We have no competing interests

Authors' Contributions

M.A.S. wrote the manuscript initial draft, conducted fieldwork/sampling, compiled datasets and carried out bulk and organic geochemical analyses. J.C.F. provided inorganic XRF data, conducted fieldwork/sampling, contributed ideas on sedimentology and to the initial manuscript. L.L.A. carried out microbiological analyses. F.S.F. advised on suitable organic geochemical techniques and provided insight into OM reactivity. N.D.G. designed microbiological approach and contributed key ideas on redox stratification to initial manuscript. K.T. carried out quantitative 16S rRNA analyses and co-designed microbiological approach. K.R.H project managed ¹⁴C radiocarbon analyses. R.G.H carried out $\delta^{15}\text{N}$ analyses with M.A.S. and advised on geochemical sampling strategy. S.F.H. & A.T. carried out fieldwork & porewater nutrient analysis which underpins model comparison. P.L. carried out bioinformatics and constructed sequencing pipeline. S.P. carried out ¹⁴C analyses on foraminifera. A.F. carried out grain size analysis. C.M. conducted fieldwork/sampling, advised on sedimentology and project managed inorganic geochemical aspects. G.D.A. contributed early ideas, revised the initial manuscript and project managed organic geochemical aspects. All authors commented on the manuscript and approved the final submission.

697

References

- [1] LaRowe, D. E., Arndt, S., Bradley, J. A., Estes, E. R., Hoarfrost, A., Lang, S. Q., Lloyd, K. G., Mahmoudi, N., Orsi, W. D., Shah Walter, S. R., et al. 2020 The fate of organic carbon in marine sediments - New insights from recent data and analysis. *Earth-Sci. Rev.* **204**, 103146. (DOI:10.1016/j.earscirev.2020.103146).
- [2] Bourgeois, S., Archambault, P. & Witte, U. 2017 Organic matter remineralization in marine sediments: A Pan-Arctic synthesis. *Global Biogeochemical Cycles* **31**, 190-213. (DOI:10.1002/2016gb005378).
- [3] Ravenschlag, K., Sahm, K., Pernthaler, J. & Amann, R. 1999 High Bacterial Diversity in Permanently Cold Marine Sediments. *Appl. Environ. Microbiol.* **65**, 3982-3989.
- [4] Renaud, P. E., Sejr, M. K., Bluhm, B. A., Sirenko, B. & Ellingsen, I. H. 2015 The future of Arctic benthos: Expansion, invasion, and biodiversity. *Prog. Oceanogr.* **139**, 244-257. (DOI:10.1016/j.pocean.2015.07.007).
- [5] Arrigo, K. R. & van Dijken, G. L. 2015 Continued increases in Arctic Ocean primary production. *Prog. Oceanogr.* **136**, 60-70. (DOI:10.1016/j.pocean.2015.05.002).
- [6] Boetius, A., Albrecht, S., Bakker, K., Bienhold, C., Felden, J., Fernández-Méndez, M., Hendricks, S., Katlein, C., Lalande, C., Krumpen, T., et al. 2013 Export of Algal Biomass from the Melting Arctic Sea Ice. *Science* **339**, 1430-1432. (DOI:10.1126/science.1231346).
- [7] Smith, R. W., Bianchi, T. S., Allison, M., Savage, C. & Galy, V. 2015 High rates of organic carbon burial in fjord sediments globally. *Nature Geoscience* **8**, 450-453. (DOI:10.1038/ngeo2421).
- [8] Hedges, J. I., Keil, R. G. & Benner, R. 1997 What happens to terrestrial organic matter in the ocean? *Organic Geochemistry* **27**, 195-212. (DOI:10.1016/S0146-6380(97)00066-1).
- [9] Stein, R., Macdonald, R. W., Stein, R. & MacDonald, R. W. 2004 The organic carbon cycle in the Arctic Ocean.
- [10] Wakeham, S. G. & Canuel, E. A. 2006 Degradation and Preservation of Organic Matter in Marine Sediments. In *Marine Organic Matter: Biomarkers, Isotopes and DNA* (ed. J. K. Volkman), pp. 295-321. Berlin, Heidelberg, Springer Berlin Heidelberg.
- [11] Arndt, S., Jørgensen, B. B., LaRowe, D. E., Middelburg, J. J., Pancost, R. D. & Regnier, P. 2013 Quantifying the degradation of organic matter in marine sediments: A review and synthesis. *Earth-Sci. Rev.* **123**, 53-86. (DOI:10.1016/j.earscirev.2013.02.008).
- [12] Zonneveld, K. A. F., Versteegh, G. J. M., Kasten, S., Eglinton, T. I., Emeis, K. C., Huguet, C., Koch, B. P., de Lange, G. J., de Leeuw, J. W., Middelburg, J. J., et al. 2010 Selective preservation of organic matter in marine environments; processes and impact on the sedimentary record. *Biogeosciences* **7**, 483-511. (DOI:10.5194/bg-7-483-2010).
- [13] Madureira, L. A. S., Conte, M. H. & Eglinton, G. 1995 Early diagenesis of lipid biomarker compounds in North Atlantic sediments. *Paleoceanography* **10**, 627-642. (DOI:10.1029/94pa03299).
- [14] Ravenschlag, K., Sahm, K. & Amann, R. 2001 Quantitative Molecular Analysis of the Microbial Community in Marine Arctic Sediments (Svalbard). *Appl. Environ. Microbiol.* **67**, 387-395. (DOI:10.1128/aem.67.1.387-395.2001).
- [15] Jørgensen, S. L., Hannisdal, B., Lanzén, A., Baumberger, T., Flesland, K., Fonseca, R., Øvreås, L., Steen, I. H., Thorseth, I. H., Pedersen, R. B., et al. 2012 Correlating microbial community profiles with geochemical data in highly stratified sediments from the Arctic Mid-Ocean Ridge. *Proceedings of the National Academy of Sciences* **109**, E2846-E2855. (DOI:10.1073/pnas.1207574109).
- [16] Algora, C., Gründger, F., Adrian, L., Damm, V., Richnow, H.-H. & Krüger, M. 2013 Geochemistry and Microbial Populations in Sediments of the Northern Baffin Bay, Arctic. *Geomicrobiol. J.* **30**, 690-705. (DOI:10.1080/01490451.2012.758195).
- [17] Jones, J. G. 1985 Microbes and microbial processes in sediments. *Philosophical Transactions of the Royal Society of London. Series A, Mathematical and Physical Sciences* **315**, 3-17. (DOI:10.1098/rsta.1985.0025).

- [18] van der Weijden, C. H., Reichart, G. J. & Visser, H. J. 1999 Enhanced preservation of organic matter in sediments deposited within the oxygen minimum zone in the northeastern Arabian Sea. *Deep Sea Research Part I: Oceanographic Research Papers* **46**, 807-830. (DOI:10.1016/S0967-0637(98)00093-4).
- [19] Onarheim, I. H. & Årthun, M. 2017 Toward an ice-free Barents Sea. *Geophysical Research Letters* **44**, 8387-8395. (DOI:10.1002/2017gl074304).
- [20] Serreze, M. C., Holland, M. M. & Stroeve, J. 2007 Perspectives on the Arctic's Shrinking Sea-Ice Cover. *Science* **315**, 1533-1536. (DOI:10.1126/science.1139426).
- [21] Stroeve, J. C., Kattsov, V., Barrett, A., Serreze, M., Pavlova, T., Holland, M. & Meier, W. N. 2012 Trends in Arctic sea ice extent from CMIP5, CMIP3 and observations. *Geophysical Research Letters* **39**, 1-7. (DOI:10.1029/2012GL052676).
- [22] Serreze, M. C. & Barry, R. G. 2011 Processes and impacts of Arctic amplification: A research synthesis. *Global Planet. Change* **77**, 85-96. (DOI:10.1016/j.gloplacha.2011.03.004).
- [23] Polyakov, I. V., Pnyushkov, A. V., Alkire, M. B., Ashik, I. M., Baumann, T. M., Carmack, E. C., Goszczko, I., Guthrie, J., Ivanov, V. V., Kanzow, T., et al. 2017 Greater role for Atlantic inflows on sea-ice loss in the Eurasian Basin of the Arctic Ocean. *Science* **356**, 285-291. (DOI:10.1126/science.aai8204).
- [24] Ardyna, M., Babin, M., Gosselin, M., Devred, E., Rainville, L. & Tremblay, J.-É. 2014 Recent Arctic Ocean sea ice loss triggers novel fall phytoplankton blooms. *Geophysical Research Letters* **41**, 6207-6212. (DOI:10.1002/2014gl061047).
- [25] Lind, S., Ingvaldsen, R. B. & Furevik, T. 2018 Arctic warming hotspot in the northern Barents Sea linked to declining sea-ice import. *Nature Climate Change* **8**, 634-639. (DOI:10.1038/s41558-018-0205-y).
- [26] Jacob, M., Soltwedel, T., Boetius, A. & Ramette, A. 2013 Biogeography of Deep-Sea Benthic Bacteria at Regional Scale (LTER HAUSGARTEN, Fram Strait, Arctic). *PloS one* **8**, e72779. (DOI:10.1371/journal.pone.0072779).
- [27] Algora, C., Vasileiadis, S., Wasmund, K., Trevisan, M., Krüger, M., Puglisi, E. & Adrian, L. 2015 Manganese and iron as structuring parameters of microbial communities in Arctic marine sediments from the Baffin Bay. *FEMS Microbiol. Ecol.* **91**. (DOI:10.1093/femsec/fiv056).
- [28] Bienhold, C., Boetius, A. & Ramette, A. 2012 The energy–diversity relationship of complex bacterial communities in Arctic deep-sea sediments. *The ISME Journal* **6**, 724-732. (DOI:10.1038/ismej.2011.140).
- [29] Freitas, F. S., Hendry, K. R., Henley, S. F., Faust, J. C., Tessin, A. C., Stevenson, M. A., Abbott, G. D., März, C. & Arndt, S. 2020 Benthic-pelagic coupling in the Barents Sea: an integrated data-model framework. *Philosophical Transactions of the Royal Society A*.
- [30] Hopkins, J. 2018 The Changing Arctic Ocean Cruise JR16006. In *RRS James Clark Ross Cruise Report No. 51 30 June - 8 August 2017* (Liverpool, National Oceanography Centre).
- [31] Stevenson, M. A. & Abbott, G. D. 2019 Exploring the composition of macromolecular organic matter in Arctic Ocean sediments under a changing sea ice gradient. *Journal of Analytical and Applied Pyrolysis* **140**, 102-111. (DOI:10.1016/j.jaap.2019.02.006).
- [32] Fetterer, F., Knowles, K., Meier, W., Savoie, M. & Windnagel, A. 2017 Updated daily. Sea Ice Index, Version 3, Boulder, Colorado USA. NSIDC: National Snow and Ice Data Center. (
- [33] Holtvoeth, J., Vogel, H., Wagner, B. & Wolff, G. A. 2010 Lipid biomarkers in Holocene and glacial sediments from ancient Lake Ohrid (Macedonia, Albania). *Biogeosciences* **7**, 3473-3489. (DOI:10.5194/bg-7-3473-2010).
- [34] Bourbonniere, R. A. & Meyers, P. A. 1996 Sedimentary geolipid records of historical changes in the watersheds and productivities of Lakes Ontario and Erie. *Limnology and Oceanography* **41**, 352-359. (DOI:10.4319/lo.1996.41.2.0352).
- [35] Matsuda, H. & Koyama, T. 1977 Early diagenesis of fatty acids in lacustrine sediments—II. A statistical approach to changes in fatty acid composition from recent sediments and some source materials. *Geochimica et Cosmochimica Acta* **41**, 1825-1834. (DOI:10.1016/0016-7037(77)90214-9).

- [36] Bray, E. E. & Evans, E. D. 1961 Distribution of *n*-paraffins as a clue to recognition of source beds. *Geochimica et Cosmochimica Acta* **22**, 2-15. (DOI:10.1016/0016-7037(61)90069-2).
- [37] Scalan, E. S. & Smith, J. E. 1970 An improved measure of the odd-even predominance in the normal alkanes of sediment extracts and petroleum. *Geochimica et Cosmochimica Acta* **34**, 611-620. (DOI:10.1016/0016-7037(70)90019-0).
- [38] Pearson, E. J., Farrimond, P. & Juggins, S. 2007 Lipid geochemistry of lake sediments from semi-arid Spain: Relationships with source inputs and environmental factors. *Organic Geochemistry* **38**, 1169-1195. (DOI:10.1016/j.orggeochem.2007.02.007).
- [39] Kozich, J. J., Westcott, S. L., Baxter, N. T., Highlander, S. K. & Schloss, P. D. 2013 Development of a Dual-Index Sequencing Strategy and Curation Pipeline for Analyzing Amplicon Sequence Data on the MiSeq Illumina Sequencing Platform. *Appl. Environ. Microbiol.* **79**, 5112-5120. (DOI:10.1128/aem.01043-13).
- [40] Caporaso, J. G., Lauber, C. L., Walters, W. A., Berg-Lyons, D., Lozupone, C. A., Turnbaugh, P. J., Fierer, N. & Knight, R. 2011 Global patterns of 16S rRNA diversity at a depth of millions of sequences per sample. *Proceedings of the National Academy of Sciences* **108**, 4516-4522. (DOI:10.1073/pnas.1000080107).
- [41] Bolyen, E. & Rideout, J. R. & Dillon, M. R. & Bokulich, N. A. & Abnet, C. C. & Al-Ghalith, G. A. & Alexander, H. & Alm, E. J. & Arumugam, M. & Asnicar, F., et al. 2019 Reproducible, interactive, scalable and extensible microbiome data science using QIIME 2. *Nat. Biotechnol.* **37**, 852-857. (DOI:10.1038/s41587-019-0209-9).
- [42] Callahan, B. J., McMurdie, P. J., Rosen, M. J., Han, A. W., Johnson, A. J. A. & Holmes, S. P. 2016 DADA2: High-resolution sample inference from Illumina amplicon data. *Nat. Methods* **13**, 581-583. (DOI:10.1038/nmeth.3869).
- [43] Quast, C., Pruesse, E., Yilmaz, P., Gerken, J., Schweer, T., Yarza, P., Peplies, J. & Glöckner, F. O. 2012 The SILVA ribosomal RNA gene database project: improved data processing and web-based tools. *Nucleic Acids Res.* **41**, D590-D596. (DOI:10.1093/nar/gks1219).
- [44] Ovreås, L., Forney, L., Daae, F. L. & Torsvik, V. 1997 Distribution of bacterioplankton in meromictic Lake Saelenvannet, as determined by denaturing gradient gel electrophoresis of PCR-amplified gene fragments coding for 16S rRNA. *Appl. Environ. Microbiol.* **63**, 3367-3373.
- [45] Suzuki, M. T., Taylor, L. T. & DeLong, E. F. 2000 Quantitative Analysis of Small-Subunit rRNA Genes in Mixed Microbial Populations via 5'-Nuclease Assays. *Appl. Environ. Microbiol.* **66**, 4605-4614. (DOI:10.1128/aem.66.11.4605-4614.2000).
- [46] Currie, A. R., Tait, K., Parry, H., de Francisco-Mora, B., Hicks, N., Osborn, A. M., Widdicombe, S. & Stahl, H. 2017 Marine Microbial Gene Abundance and Community Composition in Response to Ocean Acidification and Elevated Temperature in Two Contrasting Coastal Marine Sediments. *Frontiers in Microbiology* **8**. (DOI:10.3389/fmicb.2017.01599).
- [47] Tuna, T., Fagault, Y., Bonvalot, L., Capano, M. & Bard, E. 2018 Development of small CO₂ gas measurements with AixMICADAS. *Nuclear Instruments and Methods in Physics Research Section B: Beam Interactions with Materials and Atoms* **437**, 93-97. (DOI:10.1016/j.nimb.2018.09.012).
- [48] Lougheed, B. & Obrochta, S. 2016 MatCal: Open source Bayesian 14 C age calibration in MatLab. *Journal of Open Research Software* **4**. (DOI:doi.org/10.5334/jors.130).
- [49] Baskaran, M., Bianchi, T. S. & Filley, T. R. 2017 Inconsistencies between 14C and short-lived radionuclides-based sediment accumulation rates: Effects of long-term remineralization. *J. Environ. Radioact.* **174**, 10-16. (DOI:10.1016/j.jenvrad.2016.07.028).
- [50] Solan, M., Ward, E. R., Wood, C. L., Reed, A. J., Grange, L. J. & Godbold, J. A. 2020 Climate driven benthic invertebrate activity and biogeochemical functioning across the Barents Sea Polar Front. *Philosophical Transactions of the Royal Society A*.
- [51] Solan, M., Wigham, B., D., Hudson, I., R., Kennedy, R., Coulon, C., H., Norling, K., Nilsson, H., C. & Rosenberg, R. 2004 In situ quantification of bioturbation using time lapse fluorescent sediment profile imaging (f SPI), luminophore tracers and model simulation. *Mar. Ecol. Prog. Ser.* **271**, 1-12. (DOI:10.3354/meps271001).

- [52] Hale, R., Mavrogordato, M. N., Tolhurst, T. J. & Solan, M. 2014 Characterizations of how species mediate ecosystem properties require more comprehensive functional effect descriptors. *Scientific Reports* **4**, 6463. (DOI:10.1038/srep06463).
- [53] Ter Braak, C. & Smilauer, P. 2002 Canoco for Windows version 4.5. *Biometris-Plant Research International, Wageningen*.
- [54] Li, L., Kato, C. & Horikoshi, K. 1999 Bacterial diversity in deep-sea sediments from different depths. *Biodiversity & Conservation* **8**, 659-677. (DOI:10.1023/a:1008848203739).
- [55] Dyksma, S., Bischof, K., Fuchs, B. M., Hoffmann, K., Meier, D., Meyerdierks, A., Pjevac, P., Probandt, D., Richter, M., Stepanauskas, R., et al. 2016 Ubiquitous Gammaproteobacteria dominate dark carbon fixation in coastal sediments. *The ISME Journal* **10**, 1939-1953. (DOI:10.1038/ismej.2015.257).
- [56] Meyer, J., Akerman, N., Proskurowski, G. & Huber, J. 2013 Microbiological characterization of post-eruption "snowblower" vents at Axial Seamount, Juan de Fuca Ridge. *Frontiers in Microbiology* **4**. (DOI:10.3389/fmicb.2013.00153).
- [57] Qin, W., Martens-Habben, W., Kobelt, J. N. & Stahl, D. A. 2015 *Candidatus nitrosopumilus*. *Bergey's Manual of Systematics of Archaea and Bacteria*, 1-9. (DOI:10.1002/9781118960608.gbm01290).
- [58] Fredrickson, J. K., Romine, M. F., Beliaev, A. S., Auchtung, J. M., Driscoll, M. E., Gardner, T. S., Nealson, K. H., Osterman, A. L., Pinchuk, G., Reed, J. L., et al. 2008 Towards environmental systems biology of *Shewanella*. *Nature Reviews Microbiology* **6**, 592-603. (DOI:10.1038/nrmicro1947).
- [59] Coates, J. D., Lonergan, D. J., Philips, E. J. P., Jenter, H. & Lovley, D. R. 1995 *Desulfuromonas palmitatis* sp. nov., a marine dissimilatory Fe(III) reducer that can oxidize long-chain fatty acids. *Arch. Microbiol.* **164**, 406-413. (DOI:10.1007/BF02529738).
- [60] Wu, M. L., de Vries, S., van Alen, T. A., Butler, M. K., Op den Camp, H. J. M., Keltjens, J. T., Jetten, M. S. M. & Strous, M. 2011 Physiological role of the respiratory quinol oxidase in the anaerobic nitrite-reducing methanotroph '*Candidatus Methyloirabilis oxyfera*'. *Microbiology* **157**, 890-898. (DOI:10.1099/mic.0.045187-0).
- [61] Kuenen, J. G. 2008 Anammox bacteria: from discovery to application. *Nature Reviews Microbiology* **6**, 320-326. (DOI:10.1038/nrmicro1857).
- [62] Kuever, J., Rainey, F. & Widdel, F. 2014 The family desulfobacteraceae. In *The Prokaryotes: Deltaproteobacteria and Epsilonproteobacteria* (eds. E. Rosenberg, E. DeLong, S. Lory, E. Stackebrandt & F. Thompson), pp. 45-73, Springer Berlin Heidelberg.
- [63] Middelburg, J. J. 2018 Review and syntheses: to the bottom of carbon processing at the seafloor. *Biogeosciences* **15**, 413-427. (DOI:10.5194/bg-15-413-2018).
- [64] Freudenthal, T., Wagner, T., Wenzhöfer, F., Zabel, M. & Wefer, G. 2001 Early diagenesis of organic matter from sediments of the eastern subtropical Atlantic: evidence from stable nitrogen and carbon isotopes. *Geochimica et Cosmochimica Acta* **65**, 1795-1808. (DOI:10.1016/S0016-7037(01)00554-3).
- [65] Oleszczuk, B., Michaud, E., Morata, N., Renaud, P. E. & Kędra, M. 2019 Benthic macrofaunal bioturbation activities from shelf to deep basin in spring to summer transition in the Arctic Ocean. *Mar. Environ. Res.* **150**, 104746. (DOI:10.1016/j.marenvres.2019.06.008).
- [66] Saxena, P. B. 2007 *Chemistry of Alkaloids*. Delhi, Discovery Publishing House.
- [67] Crompton, D. W. T., Crompton, D. W. T. & Nickol, B. B. 1985 *Biology of the Acanthocephala*, Cambridge University Press.
- [68] Abbott, G. D., Lewis, C. A., Maxwell, J. R., Durand, B., Mackenzie, A. S., McKenzie, D. P., Beaumont, C., Eglinton, G., Curtis, C. D., McKenzie, D. P., et al. 1985 The kinetics of specific organic reactions in the zone of catagenesis. *Philosophical Transactions of the Royal Society of London. Series A, Mathematical and Physical Sciences* **315**, 107-122. (DOI:doi:10.1098/rsta.1985.0032).
- [69] Wen-Yen, H. & Meinschein, W. G. 1976 Sterols as source indicators of organic materials in sediments. *Geochimica et Cosmochimica Acta* **40**, 323-330. (DOI:10.1016/0016-7037(76)90210-6).

- [70] Yunker, M. B., Belicka, L. L., Harvey, H. R. & Macdonald, R. W. 2005 Tracing the inputs and fate of marine and terrigenous organic matter in Arctic Ocean sediments: A multivariate analysis of lipid biomarkers. *Deep Sea Research Part II: Topical Studies in Oceanography* **52**, 3478-3508. (DOI:10.1016/j.dsr2.2005.09.008).
- [71] Bianchi, T. S. & Canuel, E. A. 2011 *Chemical biomarkers in aquatic ecosystems*, Princeton University Press.
- [72] Vonk, J. E., van Dongen, B. E. & Gustafsson, Ö. 2008 Lipid biomarker investigation of the origin and diagenetic state of sub-arctic terrestrial organic matter presently exported into the northern Bothnian Bay. *Marine Chemistry* **112**, 1-10. (DOI:10.1016/j.marchem.2008.07.001).
- [73] Meyers, P. A. 1997 Organic geochemical proxies of paleoceanographic, paleolimnologic, and paleoclimatic processes. *Organic Geochemistry* **27**, 213-250. (DOI:10.1016/S0146-6380(97)00049-1).
- [74] Pathirana, I., Knies, J., Felix, M. & Mann, U. 2014 Towards an improved organic carbon budget for the western Barents Sea shelf. *Clim. Past* **10**, 569-587. (DOI:10.5194/cp-10-569-2014).
- [75] Schauer, R., Bienhold, C., Ramette, A. & Harder, J. 2010 Bacterial diversity and biogeography in deep-sea surface sediments of the South Atlantic Ocean. *The ISME Journal* **4**, 159-170. (DOI:10.1038/ismej.2009.106).
- [76] Han, D., Kang, I., Ha, H. K., Kim, H. C., Kim, O.-S., Lee, B. Y., Cho, J.-C., Hur, H.-G. & Lee, Y. K. 2014 Bacterial Communities of Surface Mixed Layer in the Pacific Sector of the Western Arctic Ocean during Sea-Ice Melting. *PLOS ONE* **9**, e86887. (DOI:10.1371/journal.pone.0086887).
- [77] Lipp, J. S., Morono, Y., Inagaki, F. & Hinrichs, K.-U. 2008 Significant contribution of Archaea to extant biomass in marine subsurface sediments. *Nature* **454**, 991-994. (DOI:10.1038/nature07174).
- [78] Parkes, R. J., Cragg, B. A. & Wellsbury, P. 2000 Recent studies on bacterial populations and processes in subseafloor sediments: A review. *HydJ* **8**, 11-28. (DOI:10.1007/pl00010971).
- [79] Walsh, E. A., Kirkpatrick, J. B., Pockalny, R., Sauvage, J., Spivack, A. J., Murray, R. W., Sogin, M. L. & D'Hondt, S. 2016 Relationship of Bacterial Richness to Organic Degradation Rate and Sediment Age in Subseafloor Sediment. *Appl. Environ. Microbiol.* **82**, 4994-4999. (DOI:10.1128/aem.00809-16).
- [80] Könneke, M., Bernhard, A. E., de la Torre, J. R., Walker, C. B., Waterbury, J. B. & Stahl, D. A. 2005 Isolation of an autotrophic ammonia-oxidizing marine archaeon. *Nature* **437**, 543-546. (DOI:10.1038/nature03911).
- [81] Kaneda, T. 1991 Iso- and anteiso-fatty acids in bacteria: biosynthesis, function, and taxonomic significance. *Microbiological Reviews* **55**, 288-302.
- [82] Zou, L., Wang, X.-C., Callahan, J., Culp, R. A., Chen, R. F., Altabet, M. A. & Sun, M.-Y. 2004 Bacterial roles in the formation of high-molecular-weight dissolved organic matter in estuarine and coastal waters: Evidence from lipids and the compound-specific isotopic ratios. *Limnology and Oceanography* **49**, 297-302. (DOI:10.4319/lo.2004.49.1.0297).
- [83] Cooper, W. J. & Blumer, M. 1968 Linear, iso and anteiso fatty acids in recent sediments of the North Atlantic. *Deep Sea Research and Oceanographic Abstracts* **15**, 535-540. (DOI:10.1016/0011-7471(68)90062-4).
- [84] Sáenz, J. P., Grosser, D., Bradley, A. S., Lagny, T. J., Lavrynenko, O., Broda, M. & Simons, K. 2015 Hopanoids as functional analogues of cholesterol in bacterial membranes. *Proceedings of the National Academy of Sciences* **112**, 11971-11976. (DOI:10.1073/pnas.1515607112).
- [85] Nakatsuka, T., Handa, N., Harada, N., Sugimoto, T. & Imaizumi, S. 1997 Origin and decomposition of sinking particulate organic matter in the deep water column inferred from the vertical distributions of its $\delta^{15}\text{N}$, $\delta^{13}\text{C}$ and $\delta^{14}\text{C}$. *Deep Sea Research Part I: Oceanographic Research Papers* **44**, 1957-1979. (DOI:10.1016/S0967-0637(97)00051-4).
- [86] Di Christina, T. J. & De Long, E. F. 1993 Design and application of rRNA-targeted oligonucleotide probes for the dissimilatory iron- and manganese-reducing bacterium *Shewanella putrefaciens*. *Appl. Environ. Microbiol.* **59**, 4152-4160.

- [87] Gobeil, C., Macdonald, R. W. & Sundby, B. 1997 Diagenetic separation of cadmium and manganese in suboxic continental margin sediments. *Geochimica et Cosmochimica Acta* **61**, 4647-4654. (DOI:10.1016/S0016-7037(97)00255-X).
- [88] Buongiorno, J., Herbert, L. C., Wehrmann, L. M., Michaud, A. B., Laufer, K., Røy, H., Jørgensen, B. B., Szykiewicz, A., Faiia, A., Yeager, K. M., et al. 2019 Complex Microbial Communities Drive Iron and Sulfur Cycling in Arctic Fjord Sediments. *Appl. Environ. Microbiol.* **85**, e00949-00919. (DOI:10.1128/aem.00949-19).
- [89] Llobet-Brossa, E., Rabus, R., Böttcher, M. E., Könneke, M., Finke, N., Schramm, A., Meyer, R. L., Grötzschel, S., Rosselló-Mora, R. & Amann, R. 2002 Community structure and activity of sulfate-reducing bacteria in an intertidal surface sediment: a multi-method approach. *Aquat. Microb. Ecol.* **29**, 211-226. (DOI:10.3354/ame029211).
- [90] Versantvoort, W., Guerrero-Cruz, S., Speth, D. R., Frank, J., Gambelli, L., Cremers, G., van Alen, T., Jetten, M. S. M., Kartal, B., Op den Camp, H. J. M., et al. 2018 Comparative Genomics of Candidatus Methylomirabilis Species and Description of Ca. Methylomirabilis Lanthanidiphila. *Frontiers in Microbiology* **9**. (DOI:10.3389/fmicb.2018.01672).
- [91] Chen, J., Jiang, X.-W. & Gu, J.-D. 2015 Existence of Novel Phylotypes of Nitrite-Dependent Anaerobic Methane-Oxidizing Bacteria in Surface and Subsurface Sediments of the South China Sea. *Geomicrobiol. J.* **32**, 1-10. (DOI:10.1080/01490451.2014.917742).
- [92] Martinez-Cruz, K., Leewis, M.-C., Herriott, I. C., Sepulveda-Jauregui, A., Anthony, K. W., Thalasso, F. & Leigh, M. B. 2017 Anaerobic oxidation of methane by aerobic methanotrophs in sub-Arctic lake sediments. *Sci. Total Environ.* **607-608**, 23-31. (DOI:10.1016/j.scitotenv.2017.06.187).
- [93] Zhou, L., Wang, Y., Long, X.-E., Guo, J. & Zhu, G. 2014 High abundance and diversity of nitrite-dependent anaerobic methane-oxidizing bacteria in a paddy field profile. *FEMS Microbiol. Lett.* **360**, 33-41. (DOI:10.1111/1574-6968.12567).
- [94] Mayer, L. M. 1993 Organic Matter at the Sediment-Water Interface. In *Organic Geochemistry: Principles and Applications* (eds. M. H. Engel & S. A. Macko), pp. 171-184. Boston, MA, Springer US.
- [95] Aller, R. C. & Cochran, J. K. 2019 The Critical Role of Bioturbation for Particle Dynamics, Priming Potential, and Organic C Remineralization in Marine Sediments: Local and Basin Scales. *Frontiers in Earth Science* **7**. (DOI:10.3389/feart.2019.00157).
- [96] Rasmussen, T. L. & Thomsen, E. 2013 Pink marine sediments reveal rapid ice melt and Arctic meltwater discharge during Dansgaard-Oeschger warmings. *Nature Communications* **4**, 2849. (DOI:10.1038/ncomms3849).
- [97] Thomsen, C., Blaume, F., Fohrmann, H., Peeken, I. & Zeller, U. 2001 Particle transport processes at slope environments — event driven flux across the Barents Sea continental margin. *Mar. Geol.* **175**, 237-250. (DOI:10.1016/S0025-3227(01)00143-8).
- [98] Hood, E., Fellman, J., Spencer, R. G. M., Hernes, P. J., Edwards, R., D'Amore, D. & Scott, D. 2009 Glaciers as a source of ancient and labile organic matter to the marine environment. *Nature* **462**, 1044. (DOI:10.1038/nature08580).
- [99] Bhatia, M. P., Das, S. B., Xu, L., Charette, M. A., Wadham, J. L. & Kujawinski, E. B. 2013 Organic carbon export from the Greenland ice sheet. *Geochimica et Cosmochimica Acta* **109**, 329-344. (DOI:10.1016/j.gca.2013.02.006).
- [100] Deng, L., Bülsterli, D., Kristensen, E., Meile, C., Su, C.-C., Bernasconi, S. M., Seidenkrantz, M.-S., Glombitza, C., Lagostina, L., Han, X., et al. 2020 Macrofaunal control of microbial community structure in continental margin sediments. *Proceedings of the National Academy of Sciences* **117**, 15911-15922. (DOI:10.1073/pnas.1917494117).
- [101] Faust, J. C., Stevenson, M. A., Abbott, G. D., Knies, J., Tessin, A., Mannion, I., Ford, A., Hilton, R., Peakall, J. & März, C. 2020 Does Arctic warming reduce preservation of organic matter in Barents Sea sediments? *Philosophical Transactions of the Royal Society A*.

[102] Barton, B. I., Lenn, Y.-D. & Lique, C. 2018 Observed atlantification of the Barents Sea causes the Polar Front to limit the expansion of winter sea ice. *Journal of Physical Oceanography* **48**, 1849–1866. (DOI:10.1175/JPO-D-18-0003.1).

Figure and table captions

Figures

Figure 1: Bulk organic, inorganic and grain size data against depth (cm) to highlight changes taking place below the sediment-water interface with age estimation at 27.5 cm depth for radiocarbon (^{14}C -AMS) on planktonic and benthic foraminifera. Bulk organic parameters include: total organic carbon (TOC), total nitrogen (N), TOC:N ratio and nitrogen stable isotopes ($\delta^{15}\text{N}$). Bulk inorganic parameters include iron (Fe), phosphorus (P) and Manganese (Mn). Grain size is plotted on a % cumulative basis, categorised in six size fractions (<2 μm , 2-63 μm , 63-128 μm , 128-250 μm , 250-500 μm , 500 - 2000 μm).

Figure 2: Organic geochemical parameters plotted against depth (cm) with $f\text{-SPL}_{\text{mean}}$ (0.5 cm, average of three replicates) and $f\text{-SPL}_{\text{max}}$ (4.3 cm, greatest of three replicates) bioturbation depths indicated, together with bioturbation activity (insert provides detail 0-4.5 cm) [50]. For *n*-alkanoic acids parameters include total FAMEs (fatty acid methyl esters), ratio of the C_{15} anteiso/ C_{16} FAME, terrigenous to aquatic fatty acid ratio (TAR_{FA}) [34] and total carbon preference index (CPI_{T}) [35]. For sterols parameters include cholesterol/brassicasterol, cholesterol/ β -sitosterol, stigmasterol/stigmastanol and β -sitosterol/stigmastanol. For *n*-alkanes parameters include carbon preference index (CPI) [36] and odd over even predominance for *n*- C_{17-21} & *n*- C_{21-25} (OEP_{17-21} & OEP_{21-25}) [37]. For *n*-alkanols parameters include terrestrial to aquatic ratio (TAR) and Aut/All (autochthonous/allochthonous) ratio [38].

Figure 3: Microbial parameters plotted against depth (cm) with mean and maximum bioturbation depths indicated, bioturbation activity (insert provides detail 0-4.5 cm) [50], coincident pore-water oxygen transition [29] and modeled relative contribution of metabolic pathway to OM heterotrophic degradation [29]. Microbial parameters include 16s RNA bacteria, 16s RNA archaea, *Nitrosopumilaceae*, *Shewanellaceae*, *Desulfuromonadales*, *Methylomirabilaceae*, and *Desulfobacteraceae*. Modeled data include relative aerobic respiration, denitrification, iron reduction, sulfate reduction and manganese reduction [29].

Figure 4: Principal components analysis (PCA) of bulk organic, inorganic, organic geochemical, geomicrobiological and modeled processes [29] based on \log^{10} transformed and centred datasets. Samples within the uppermost oxic and bioturbated layer [50] to ~4.5 cm depth are indicated by blue circles with deeper layers indicated by red circles.

1
2
3
4
5
6
7 **Supplements**
8

9 **Supplementary Table S1** – Summary of analyses and purpose for cores from B15.

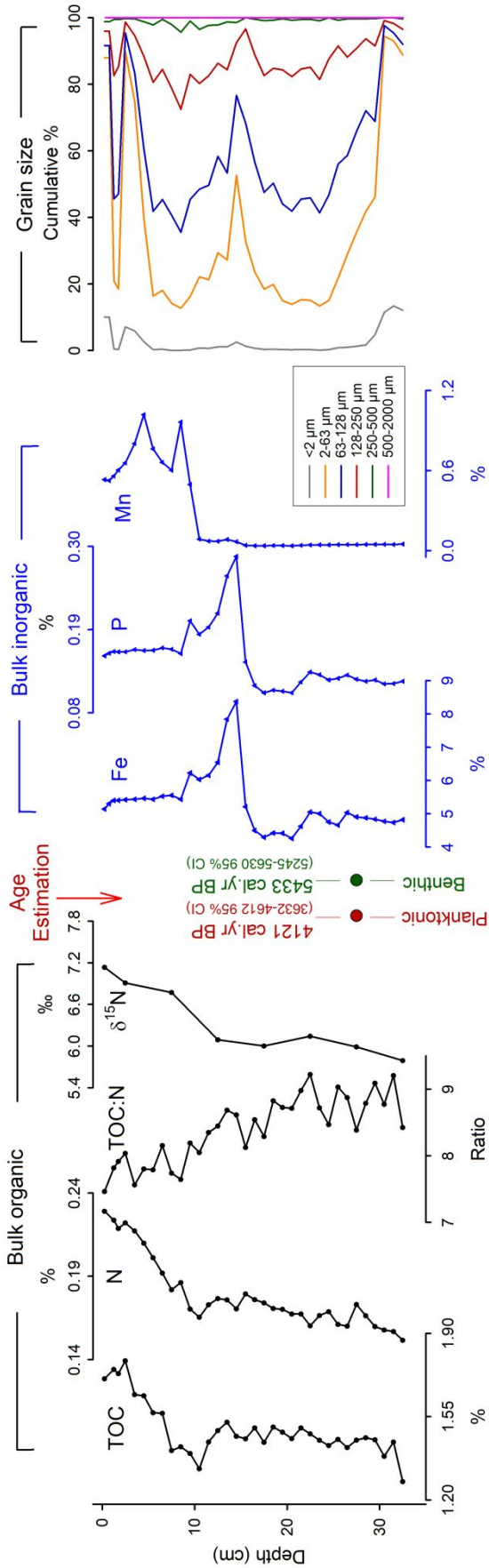
10
11 **Supplementary Figures S1 – S7** – Map of study location in the Barents Sea, correlations
12 between key geochemical, modeled and measured datasets. PCA axis 1 & 2 scores plotted
13 against depth.
14

15 **Supplementary information datasets** – Datasets utilised within this study.
16
17
18
19
20
21
22
23
24
25
26
27
28
29
30
31
32
33
34
35
36
37
38
39
40
41
42
43
44
45
46
47
48
49
50
51
52
53
54
55
56
57
58
59
60

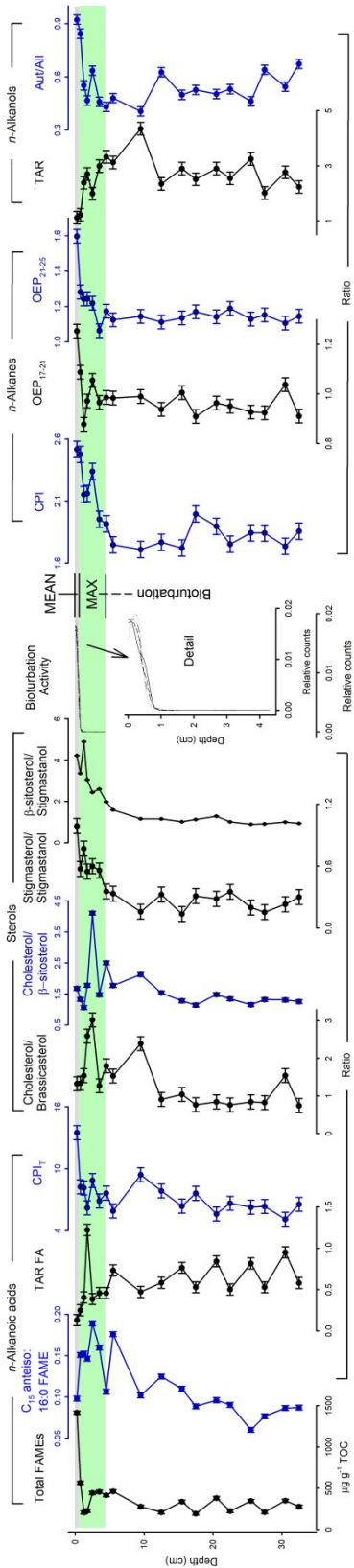
For Review Only

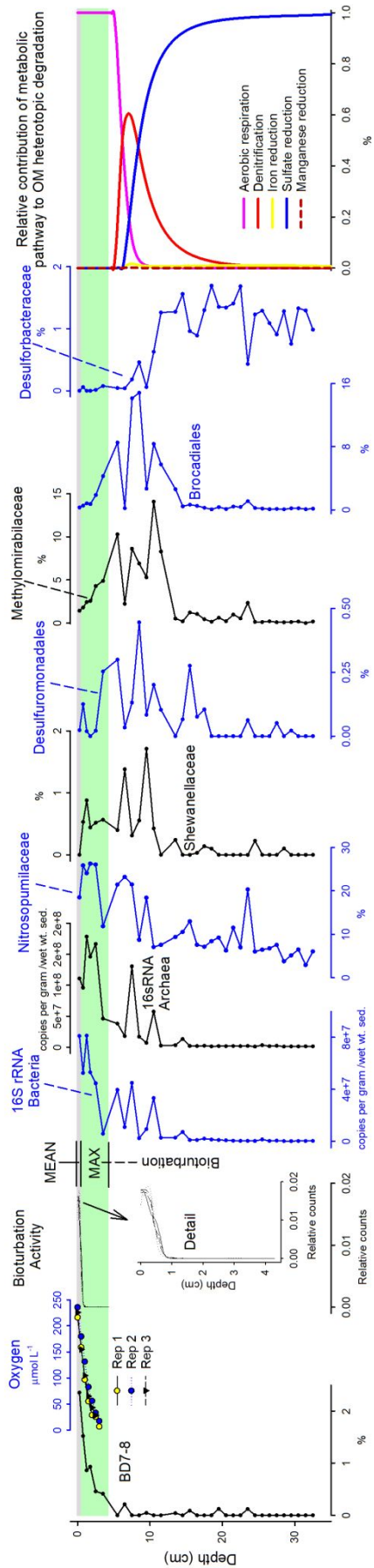
1
2
3
4
5
6
7
8
9
10
11
12
13
14
15
16
17
18
19
20
21
22
23
24
25
26
27
28
29
30
31
32
33
34
35
36
37
38
39
40
41
42
43
44
45
46
47
48
49
50
51
52
53
54
55
56
57
58
59
60

For Review Only

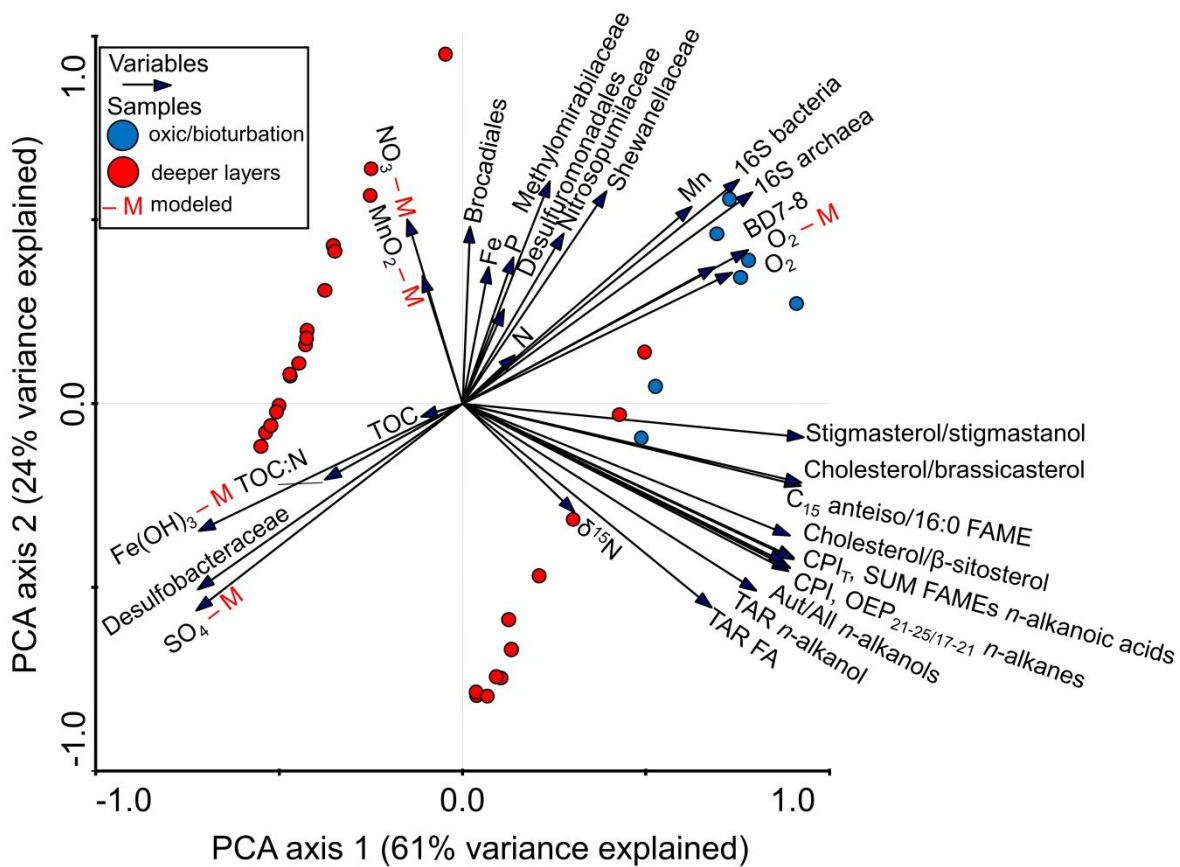


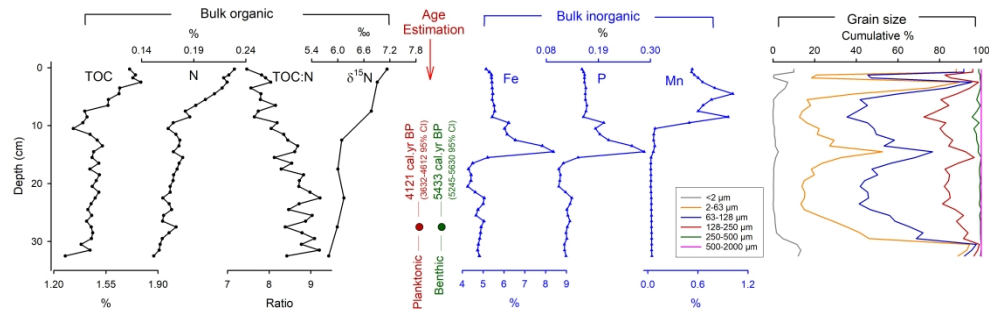
view Only





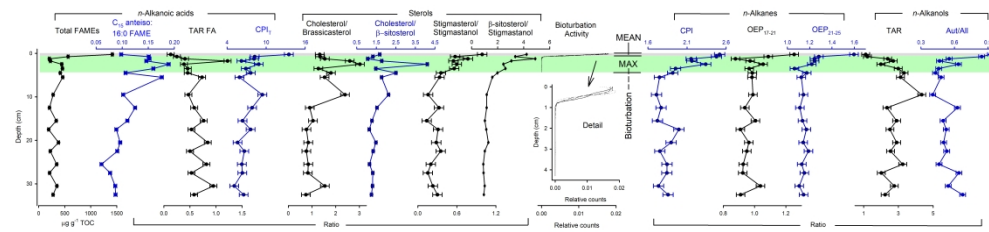
Review Only





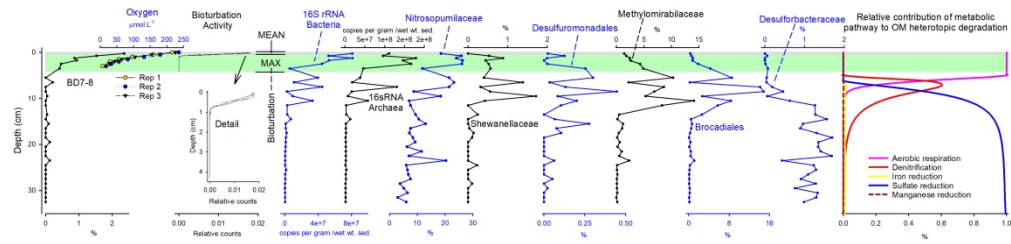
Bulk organic, inorganic and grain size data against depth (cm) to highlight changes taking place below the sediment-water interface with age estimation at 27.5 cm depth for radiocarbon (^{14}C -AMS) on planktonic and benthic foraminifera. Bulk organic parameters include: total organic carbon (TOC), total nitrogen (N), TOC:N ratio and nitrogen stable isotopes ($\delta^{15}\text{N}$). Bulk inorganic parameters include iron (Fe), phosphorus (P) and Manganese (Mn). Grain size is plotted on a % cumulative basis, categorised in six size fractions (<2 μm , 2-63 μm , 63-128 μm , 128-250 μm , 250-500 μm , 500 - 2000 μm).

479x149mm (300 x 300 DPI)



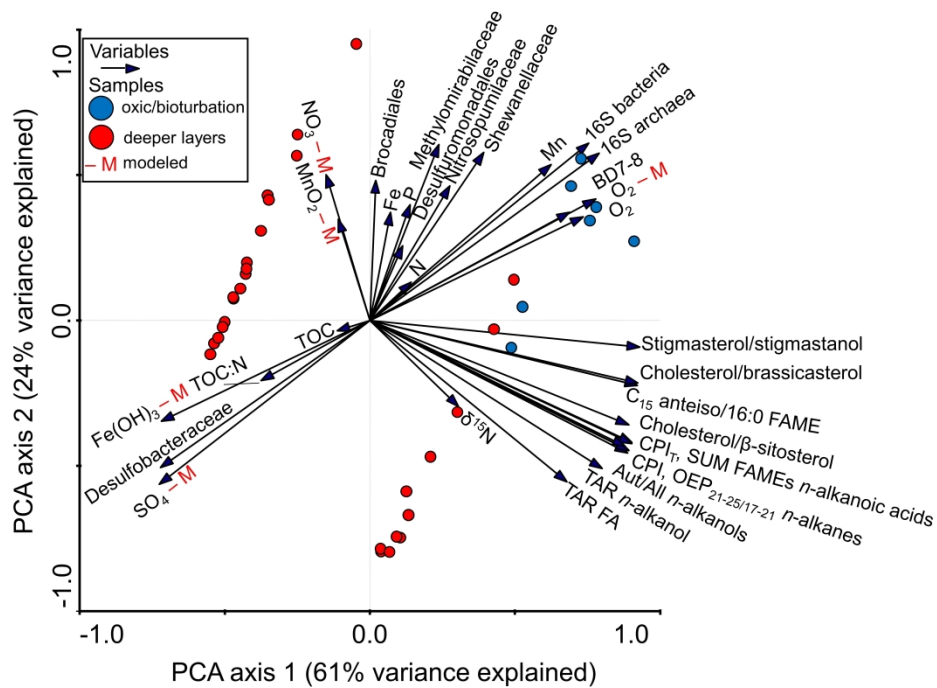
Organic geochemical parameters plotted against depth (cm) with $f\text{-SPI}_{L\text{mean}}$ (0.5 cm, average of three replicates) and $f\text{-SPI}_{L\text{max}}$ (4.3 cm, greatest of three replicates) bioturbation depths indicated, together with bioturbation activity (insert provides detail 0-4.5 cm) [50]. For *n*-alkanoic acids parameters include total FAMES (fatty acid methyl esters), ratio of the C₁₅ anteiso/C₁₆ FAME, terrigenous to aquatic fatty acid ratio (TAR_{FA}) [34] and total carbon preference index (CPI_T) [35]. For sterols parameters include cholesterol/brassicasterol, cholesterol/ β -sitosterol, stigmasterol/stigmastanol and β -sitosterol/stigmastanol. For *n*-alkanes parameters include carbon preference index (CPI) [36] and odd over even predominance for *n*-C₁₇₋₂₁ & *n*-C₂₁₋₂₅ (OEP₁₇₋₂₁ & 21-25) [37]. For *n*-alkanols parameters include terrestrial to aquatic ratio (TAR) and Aut/All (autochthonous/allochthonous) ratio [38].

639x149mm (300 x 300 DPI)



Microbial parameters plotted against depth (cm) with mean and maximum bioturbation depths indicated, bioturbation activity (insert provides detail 0-4.5 cm) [50], coincident pore-water oxygen transition [29] and modeled relative contribution of metabolic pathway to OM heterotrophic degradation [29]. Microbial parameters include 16s RNA bacteria, 16s RNA archaea, Nitrosopumilaceae, Shewanellaceae, Desulfuromonadales, Methylospiraceae, and Desulfobacteraceae. Modeled data include relative aerobic respiration, denitrification, iron reduction, sulfate reduction and manganese reduction [29].

600x149mm (150 x 150 DPI)



Principal components analysis (PCA) of bulk organic, inorganic, organic geochemical, geomicrobiological and modeled processes [29] based on \log^{10} transformed and centred datasets. Samples within the uppermost oxic and bioturbated layer [50] to ~ 4.5 cm depth are indicated by blue circles with deeper layers indicated by red circles.

1746x1251mm (96 x 96 DPI)